JVI Accepted Manuscript Posted Online 1 August 2018
J. Virol. doi:10.1128/JVI.00902-18

Inhibition of stress granule formation by Middle East respiratory syndrome coronavirus 4a accessory protein facilitates viral translation, leading to efficient virus replication

Keisuke Nakagawa[1], Krishna Narayanan[1], Masami Wada[1] and Shinji Makino[1,2,3,4,5,#]

Department of Microbiology and Immunology[1], Center for Biodefense and Emerging Infectious Diseases[2], UTMB Center for Tropical Diseases[3], Sealy Center for Vaccine Development[4], and The Institute for Human Infections and Immunity[5], The University of Texas Medical Branch, Galveston, Texas, 77555-1019

Short title: SG formation inhibition in MERS-CoV replication

#: Corresponding author: Shinji Makino

Corresponding author's Mailing Address: 4.142E Medical Research Building 301 University Boulevard, Galveston, Texas 77555-1019

Tel/Fax: (409) 775-2323/(409) 772-5065

E-mail: shmakino@utmb.edu

Abstract: 244 words, Importance: 145 words

Abstract

Stress granule (SG) formation is generally triggered as a result of stress-induced translation arrest. The impact of SG formation on virus replication varies among different viruses, and the significance of SGs in coronavirus (CoV) replication is largely unknown. The present study examined the biological role of SGs in Middle East respiratory syndrome (MERS)-CoV replication. MERS-CoV 4a accessory protein is known to inhibit SG formation in expressed cells by binding to double-stranded RNAs and inhibiting protein kinase R (PKR)-mediated eIF2α phosphorylation. Replication of MERS-CoV lacking genes 4a and 4b (MERS-CoV-Δp4), but not MERS-CoV, induced SG accumulation in MERS-CoV-susceptible HeLa/CD26 cells, while replication of both viruses failed to induce SGs in Vero cells, demonstrating cell type-specific differences in MERS-CoV-Δp4-induced SG formation. MERS-CoV-Δp4 replicated less efficiently than MERS-CoV in HeLa/CD26 cells and inhibition of SG formation by siRNA-mediated depletion of the SG components promoted MERS-CoV-Δp4 replication, demonstrating that SG formation was detrimental for MERS-CoV replication. Inefficient MERS-CoV-Δp4 replication was neither due to induction of type I and type III interferons nor accumulation of viral mRNAs in the SGs. Rather, it was due to inefficient translation of viral proteins, which was caused by high levels of PKR-mediated eIF2α phosphorylation and likely by confinement of various factors that are required for translation in the SGs. Finally, we established that deletion of 4a gene alone was sufficient for inducing SGs in infected cells. Our study revealed that 4a-mediated inhibition of SG formation facilitates viral translation, leading to efficient MERS-CoV replication.

Importance

Middle East respiratory syndrome coronavirus (MERS-CoV) causes respiratory failure with a high case fatality rate in patients, yet effective antivirals and vaccines are currently not available. Stress granule (SG) formation is one of the cellular stress responses to virus infection and is generally triggered as a result of stress-induced translation arrest. SGs can be beneficial or detrimental for virus replication, and the biological role of SGs in CoV infection is unclear. The present study showed that MERS-CoV 4a accessory protein, which was reported to block SG formation in expressed cells, inhibited SG formation in infected cells. Our data suggest that 4a-mediated inhibition of SG formation facilitates the translation of viral mRNAs, resulting in efficient virus replication. To our knowledge, this is the first report showing the biological significance of SG in CoV replication, and provides insight into the interplay between MERS-CoV and antiviral stress responses.

Introduction

Middle East respiratory syndrome (MERS), which was first reported in 2012, is a zoonotic disease caused by MERS coronavirus (MERS-CoV) (1). It has been suspected that the virus is of bat origin, while dromedaries serve as a reservoir and transmit the virus to human primarily in Middle Eastern countries (2-5). MERS patients suffer from fever, cough, and pneumonia, which can lead to respiratory failure (1, 6). The reported case fatality rate is approximately 36% (http://www.who.int/emergencies/mers-cov/en/). Hence, MERS-CoV represents a serious public health threat.

CoVs are enveloped viruses carrying a single-stranded positive-sense RNA genome of ~30-kb length (7-9) and are classified into four genera, alpha, beta, gamma, and delta CoVs. Replication of MERS-CoV, a beta CoV, starts with binding of the virus to a specific viral receptor, CD26 (also known as dipeptidyl peptidase 4) (10). After fusion of virus and host cell membranes, the incoming genomic RNA undergoes translation of two large polyproteins from open reading frame (ORF) 1a and from ORFs 1a and 1b, both of which are located in gene 1 (Fig. 1A). The polyproteins are processed into 16 mature nonstructural proteins (nsp1-nsp16), most of which are essential for synthesis of viral RNAs (11-13), including genome-length mRNA 1 and subgenomic mRNAs, mRNAs 2-8. Viral mRNAs have a common 3'-end, constituting a 3'-co-terminal nested set structure and the 5' end of all viral mRNAs carry a common leader sequence (14-17). Subgenomic mRNAs encode viral structural proteins and accessory proteins, including 3, 4a, 4b, and 5, the latter of which are not essential for virus replication, yet do affect viral pathogenicity (18-22).

Virus replication, which represents a stress to the cells, activates several signaling pathways, including those triggered by activated protein kinase R (PKR). Upon binding viral

90 double-stranded RNAs (dsRNAs), PKR undergoes autophosphorylation reaction that activates
91 the kinase. Activated PKR phosphorylates the eukaryotic initiation factor 2α (eIF2α) subunit
92 (23-25), which prevents the recycling of ternary complex $tRNA_i^{Met}$-GTP-eIF2 and inhibits the
93 43S translation complex formation, leading to inhibition of translation (23, 24, 26, 27). Hence,
94 PKR activation inhibits viral gene expression, contributing to host cell survival from infection.
95 The translation inhibition by eIF2α phosphorylation also leads to polysome disassembly
96 and subsequent accumulation of the mRNAs associated with stalled ribosome complexes to
97 cytoplasmic structures called stress granules (SGs) (27, 28). SGs act as dynamic microdomains;
98 once translation activities are restored, SGs are disassembled and mRNAs that have been stored
99 in the SGs can rapidly resume translation (27, 29, 30). SGs contain mRNAs bound to translation
100 factors, such as eIF4A and eIF3, and the 40S ribosomal subunit, plus many additional proteins
101 affecting mRNA functions. SG assembly is driven by aggregation-prone cellular RNA-binding
102 proteins, such as T cell internal antigen 1 (TIA-1) and Ras-GTPase activating SH3 domain
103 binding protein 1 (G3BP1) (27). Recent studies have shown localization of RIG-I-like receptors
104 (RLRs) and PKR in SGs during viral infection (31-33). It has been proposed that SGs exert
105 specific antiviral effects (34) by providing a critical platform for interactions between antiviral
106 proteins and non-self RNA ligands (31, 35, 36).
107 The impact of SG formation on virus replication varies among different viruses (37, 38).
108 Some viruses accomplish efficient replication by inhibiting SG formation via various
109 mechanisms. For instance, influenza A virus blocks SG formation by the NS1 protein, which
110 sequesters dsRNAs from PKR (39). Alphaherpes viruses blocks SG formation by impairing the
111 activation of eIF2α through the virion host shutoff protein, Us11, ICP34.5, and glycoprotein B
112 (40-43). Vaccinia virus E3L protein suppresses SG formation by binding to dsRNAs and

113 preventing PKR activation (44). Finally, picornaviruses disassemble SG by cleaving G3BP1 via
114 the activity of viral 3C proteinase (45). Some viruses induce or modulate SG formation for their
115 replication. For example, Newcastle disease virus triggers stable formation of SGs, which benefit
116 viral protein translation and virus replication by arresting cellular mRNAs (46). Vesicular
117 stomatitis virus induces SG-like structures, which contain viral RNAs and viral proteins
118 necessary for RNA synthesis, suggesting that SG-like structures are important for virus
119 replication (47, 48). Hepatitis C virus induces the assembly and disassembly of SGs in an eIF2α-
120 dependent manner and some components of SGs play a pivotal role in several steps of the virus
121 life cycle (49, 50).

122 Several past studies reported either SG formation or absence of it in the context of CoV
123 infection. Transmissible gastroenteritis coronavirus (TGEV), an alpha CoV, induces aggregation
124 of granules containing viral mRNAs associated with the polypyrimidine tract-binding protein
125 and SG markers, TIA-1 and TIAR, late in infection (51). Mouse hepatitis virus (MHV), a beta
126 CoV, induces SGs when phosphorylation of eIF2α and host translational shutoff occur (52).
127 Rabouw *et al*. reported that expression of MERS-CoV 4a protein, an accessory protein, impedes
128 PKR phosphorylation and SG formation, whereas MERS-CoV as well as MERS-CoV lacking
129 both ORFs 4a and 4b (Fig. 1A) did not induce SGs in infected cells (53). Absence of SG
130 formation in the mutant MERS-CoV-infected cells led the authors to speculate that MERS-CoV
131 encodes at least one other stress response antagonist with a mode of action that differs from that
132 of 4a (53). Currently, the biological significance of SG formation or inhibition of it during CoV
133 replication are unclear.

134 Rabouw *et al*. tested SG formation in MERS-CoV-infected Vero cells, but they used
135 HeLa cells to study 4a protein-induced SG formation (53). As PKR expression levels are low in

Vero cells (54), the extent of the PKR-induced eIF2α phosphorylation caused by the MERS-CoV mutant in Vero cells might have been too low for induction of SG formation. If this is the case, the MERS-CoV mutant would induce SGs in other cells, where PKR expression levels are high enough for inducing eIF2α phosphorylation and the extent of which is sufficient for SG formation. In the present study, we explored this possibility and found that replication of MERS-CoV mutant lacking ORFs 4a and 4b (MERS-CoV-Δp4), but not wild-type MERS-CoV (MERS-CoV-WT), induced SG formation in HeLa-derived susceptible cells. Our study further demonstrated that inhibition of SG formation facilitated translation of viral proteins, leading to efficient virus replication, and that depletion of MERS-CoV 4a protein alone was sufficient for inducing SG formation in infected cells. To our knowledge, this is the first study revealing the biological role of SGs in CoV replication and identifying a CoV protein that suppresses SG accumulation in infected cells.

Results

MERS-CoV-Δp4 infection induces SGs in HeLa/CD26 cells. To determine whether replication of MERS-CoV-Δp4 (Fig. 1A) induces SG formation, we established a HeLa cell line stably expressing the MERS-CoV receptor, human CD26 (HeLa/CD26 cells). HeLa cells express significantly higher levels of PKR than Vero cells (54). We inoculated MERS-CoV-WT or MERS-CoV-Δp4, both of which were rescued by using a reverse genetics system (55), into HeLa/CD26 cells at an MOI of 3; our MERS-CoV-Δp4 and the MERS-CoV mutant described by Rabouw *et al*. (53) have the same deletion in the gene 4. The cells were subjected to immunofluorescence analysis using specific antibodies for SG markers, TIA-1, G3BP, or eIF4A,

158 together with the MERS-CoV N protein. Granules containing these SG markers accumulated in
159 MERS-CoV-Δp4-infected cells, but not in MERS-CoV-WT-infected cells (Figs. 1B-1D).

160 SGs are dynamic structures and disperse without a source of new translation initiation
161 complexes (27-30). Cycloheximide (CHX) stalls translation, leading to dismantling of SGs (28);
162 hence, if these granules carrying the SG markers in MERS-CoV-Δp4-infected cells are indeed
163 SGs, CHX treatment would disperse them. CHX treatment, but not dimethyl sulfoxide (DMSO)
164 treatment, caused dispersion of TIA-1-positive granules in MERS-CoV-Δp4-infected cells,
165 establishing that MERS-CoV-Δp4, but not MERS-CoV-WT, induced SGs in infected
166 HeLa/CD26 cells (Fig. 1E).

167 We next determined kinetics of accumulation of SG-positive cells by counting cells
168 positive for both TIA-1 and N proteins (SG-positive cells) and those positive for only N protein
169 (SG-negative cells) at different times postinfection (p.i.); cells showing at least one SG were
170 considered to be SG-positive. Approximately 5% of MERS-CoV-Δp4-infected cells were SG-
171 positive at 6 h p.i., and the number of SG-positive cells increased as infection progressed, with
172 ~80% and ~100% at 9 h p.i. and at 12 h p.i., respectively (Fig. 1F left panel). In contrast, SG-
173 positive cells represented a very minor population in MERS-CoV-WT-infected cells throughout
174 the infection.

175 We also tested MERS-CoV-Δp4-induced SG formation in other cells. Replication of
176 MERS-CoV-WT and MERS-CoV-Δp4 did not induce SGs in Vero cells (Figs. 1F right panel,
177 1G), confirming the data shown in a previous report (53). In contrast, replication of MERS-CoV-
178 Δp4, but not MERS-CoV-WT, in 293 cells stably expressing CD26 (293/CD26 cells) (56)
179 induced SG accumulation (Fig. 1H), demonstrating that MERS-CoV-Δp4-induced SG formation

was not limited to HeLa/CD26 cells. These data showed that MERS-CoV-Δp4-induced SG formation was cell type-dependent.

Growth kinetics of MERS-CoV-WT and MERS-CoV-Δp4 in Vero and HeLa/CD26 cells. To glean whether SG formation affects virus replication, we next examined the growth kinetics of MERS-CoV-WT and MERS-CoV-Δp4 in HeLa/CD26 and Vero cells. In HeLa/CD26 cells, the titers of MERS-CoV-WT were significantly higher than those of MERS-CoV-Δp4 at 18 and 24 h p.i. at an MOI of 0.01, and were also higher at 12, 18, and 24 h p.i. at an MOI of 3 (Fig. 2A). In Vero cells, both viruses replicated similarly at an MOI of 0.01, while titers of MERS-CoV-WT were higher than those of MERS-CoV-Δp4 at 24, 36, and 48 h p.i. at an MOI of 3 (Fig. 2B). As SG formation did not occur in MERS-CoV-Δp4-infected Vero cells, the differences in virus titers among the two viruses in Vero cells were not due to SG formation. At high MOI infection, the difference in the maximum virus titers between the two viruses in Vero cells (~3.3-times at 48 h p.i.) were less prominent than in HeLa/CD26 cells (~12-times at 18 h p.i.). Considering the fact that MERS-CoV-Δp4 replication induced SGs in HeLa/CD26 cells, not in Vero cells, these results suggested that the SG formation negatively affected virus replication.

Phosphorylation status of PKR and eIF2α and translation activities in infected cells. MERS-CoV 4a protein inhibits PKR phosphorylation by binding to dsRNAs and sequestering dsRNAs from PKR (53), yet the effects of 4a on PKR activation and eIF2α phosphorylation in infected cells are unknown. We found that phosphorylation levels of PKR and eIF2α were clearly higher in HeLa/CD26 cells infected with MERS-CoV-Δp4 than in those infected with MERS-CoV-WT (Fig. 3A). In contrast, both viruses induced low levels of PKR phosphorylation

203 and eIF2α phosphorylation in Vero cells (Fig. 3B). As expected, 4a and 4b proteins accumulated
204 in MERS-CoV-WT-infected cells, but not in MERS-CoV-Δp4-infected cells (Figs. 3A and 3B).
205 Appearance of two 4a protein bands suggest that the 4a accessory protein underwent
206 modification, the nature of which is unknown, in infected cells.

207 We next investigated the extent of host and viral protein synthesis by pulse radiolabeling
208 of the cells with ^{35}S-methinone/cysteine. In HeLa/CD26 cells, both viruses clearly induced
209 translation suppression after 9 h p.i., with stronger inhibition in MERS-CoV-Δp4-infected cells
210 than in MERS-CoV-WT-infected cells (Fig. 3C). Also, the synthesis of viral-specific proteins
211 was lower in MERS-CoV-Δp4-infected cells than in MERS-CoV-WT-infected cells after 9 h p.i.
212 Thus, there was an inverse correlation between the extent of phosphorylation of PKR/eIF2α and
213 translation activities in infected HeLa/CD26 cells. In Vero cells, synthesis of virus-specific
214 proteins was notable after 24 h p.i., and levels of host protein synthesis were similar among
215 mock-infected cells, MERS-CoV-WT-infected cells, and MERS-CoV-Δp4-infected cells (Fig.
216 3D). These data imply that low levels of eIF2α phosphorylation did not inhibit host and viral
217 protein synthesis in infected Vero cells.

218 To further establish that MERS-CoV-Δp4 inhibited efficient viral protein synthesis in
219 HeLa/CD26 cells, we examined the abundance of viral mRNAs and proteins in infected
220 HeLa/CD26 cells. Northern blot analysis showed similar levels of viral mRNA accumulation
221 between MERS-CoV-WT- and MERS-CoV-Δp4-infected cells at different times p.i. (Fig. 4A).
222 Due to deletion of the ORFs 4a and 4b, mRNAs 1-3 of MERS-CoV-Δp4 migrated faster than
223 those of MERS-CoV-WT in the gel. Quantitative RT-PCR showed that mRNA 1 and mRNA 8
224 encoding N protein accumulated to similar levels in MERS-CoV-WT- and MERS-CoV-Δp4-

infected cells (Figs. 4B and 4C). These studies established that depletion of the ORFs 4a and 4b had little impact on accumulation of viral mRNAs.

Western blot analysis showed that the viral structural proteins S, M, and N, accumulated similarly in both viruses at 6 h p.i., while at 9 h p.i., when PKR-mediated eIF2α phosphorylation had occurred (Fig. 3A), the viral structural proteins accumulated to higher levels in MERS-CoV-WT-infected cells than in MERS-CoV-Δp4-infected cells (Fig. 4D). Similar results were noted at 12 h p.i. (Fig. 4D). These data established that translation of viral proteins was indeed inefficient in MERS-CoV-Δp4-infected cells.

We interpreted these data as the following: 1) MERS-CoV-Δp4 replication in HeLa/CD26 cells activated PKR, which induced eIF2α phosphorylation and strong translational suppression, leading to SG formation; 2) In MERS-CoV-WT-infected HeLa/CD26 cells, 4a-mediated inhibition of PKR activation likely prevented efficient eIF2α phosphorylation, allowing viral and host translation and preventing SG formation; 3) The PKR antagonistic function of 4a failed to show significant biological effects in Vero cells, probably due to low expression levels of PKR; and 4) Due to low levels of PKR expression, the PKR-mediated eIF2α phosphorylation was inefficient in infected Vero cells, allowing unimpeded translation of viral and host proteins and inhibiting SG formation.

Innate antiviral responses in MERS-CoV-Δp4-infected HeLa/CD26 cells. Our data supported a notion that inhibition of viral translation, which was induced by phosphorylated eIF2α, caused inefficient MERS-CoV-Δp4 replication in HeLa/CD26 cells. In addition, we suspected that SG formation itself also contributed to the inefficient MERS-CoV-Δp4 replication by one of the following mechanisms: 1) SG formation induces activation of innate immune

248 responses, leading to suppression of viral replication; 2) Viral mRNAs are stored in the SGs and
249 not available for translation, leading to inefficient viral translation; and 3) SGs store various
250 factors required for translation, e.g., translation factors and 40S ribosomal subunit, and restrict
251 availability of these factors for translation, leading to inefficient viral translation. The following
252 experiments tested these possibilities.

253 SGs provide a platform for interaction of RIG-I-like receptors and viral mRNAs, leading
254 to interferon (IFN) production (31, 35, 36). Additionally, antiviral proteins, e.g., PKR, 2′-5′-
255 oligoadenylate synthetase (OAS), and RNase L, are recruited to SGs and exert anti-viral
256 functions (31, 32). We explored whether SG formation could trigger innate immune responses by
257 examining the expression levels of *IFN-β*, *IFN-λ1*, *OAS*, and *ISG56* mRNAs in MERS-CoV-
258 WT- and MERS-CoV-Δp4-infected HeLa/CD26 cells (Fig. 5). Sendai virus (SeV), a positive
259 control, induced efficient expression of these mRNAs, while mock infection did not (Fig. 5).
260 MERS-CoV-WT or MERS-CoV-Δp4 did not induce efficient expression of these mRNAs at any
261 times p.i. Also, there were no significant differences in the expression levels of these mRNAs
262 between MERS-CoV-WT- and MERS-CoV-Δp4-infected cells. These data suggested that the
263 SGs did not play significant roles in innate immune gene expression in MERS-CoV-Δp4-
264 infected HeLa/CD26 cells.

265

266 **MERS-CoV mRNAs are not confined in the SGs.** The absence of innate immune gene
267 expression in MERS-CoV-Δp4-infected HeLa/CD26 cells may be due to the possibility that the
268 viral mRNAs are not confined in the SGs, thus escaping recognition by RIG-I-like receptors in
269 the SGs. Alternatively, viral mRNAs might have been efficiently stored in the SGs and

contributed to inefficient viral translation, yet they were unable to trigger innate immune gene expression.

To determine whether viral mRNAs are trapped in the SGs, we visualized viral mRNAs by using fluorescent *in situ* hybridization (FISH) analysis with the probe binding to all viral mRNAs. SGs were visualized by IFA staining of a SG marker, eIF4A, in mock-infected HeLa/CD26 cells, MERS-CoV-WT-infected cells, and MERS-CoV-Δp4-infected cells. eIF4A showed diffuse distribution in mock-infected cells and MERS-CoV-WT-infected cells, demonstrating absence of SG formation. Although eIF4A accumulated within SGs in MERS-CoV-Δp4-infected cells (Fig. 6), viral mRNAs were diffusely distributed in the cytoplasm in infected cells (Fig. 6). The absence of clear co-localization of viral mRNAs and eIF4A demonstrated that most of viral mRNAs were not confined in the SGs.

SG formation interferes with MERS-CoV replication. We next explored a possibility that various factors involved in translation are accumulated in the SGs, causing reduction of their abundance in the cytoplasm and leading to inefficient translation of viral proteins. If this is the case, inhibition of SG accumulation would lead to promotion of viral gene expression, as those factors involved in translation are not confined in the SGs and are available for translation. We tested this possibility by examining replication and gene expression of MERS-CoV-Δp4 in HeLa/CD26 cells that were depleted of TIA-1 or both G3BP1 and G3BP2 (G3BP1/2) by siRNA treatment. The siRNAs targeting TIA-1 and those targeting G3BP1/2 efficiently reduced levels of TIA-1 and G3BP1/2, respectively. (Fig. 7A). Depletion of TIA-1 or G3BP1/2 did not prevent SG formation in MERS-CoV-Δp4-infected cells, whereas it reduced average numbers of SGs (Fig. 7A top panels). MERS-CoV-WT replicated less efficiently in cells depleted of TIA-1 or

293 those depleted of G3BP1/2 than in control siRNA-treated cells (Fig. 7B upper-panels), implying
294 that TIA-1 and G3BP1/2 facilitated MERS-CoV replication. In contrast, MERS-CoV-Δp4
295 replicated more efficiently in TIA-1-depleted cells than in control siRNA-treated cells (Fig. 7B
296 lower left panel). Likewise, replication of MERS-CoV-Δp4 was also better in G3BP1/2-depleted
297 cells than in control siRNA-treated cells (Fig. 7B lower right panel). These data showed that the
298 reduction in the number of SGs facilitated MERS-CoV-Δp4 replication and also suggested that
299 inhibition of SG formation had more pronounced effects on promoting virus replication than the
300 positive effects of TIA-1 or G3BP1/2 for virus replication.

301 Effects of inefficient SG accumulation on translation activities were examined next.
302 Control siRNA-treated cells and TIA-1-depleted cells were first mock-infected or infected with
303 MERS-CoV-Δp4 or MERS-CoV-WT. Translational activities were then examined by metabolic
304 radiolabeling. In control siRNA-treated cells, MERS-CoV-WT and MERS-CoV-Δp4 induced
305 translational inhibition, with the latter virus showing stronger inhibition at 9 and 12 h p.i. (Fig.
306 7C). In TIA-1-depleted cells, the translation inhibitory effects caused by MERS-CoV-Δp4 were
307 less prominent at 9 and 12 h p.i. (Fig. 7C). We performed similar experiments by using cells
308 depleted of G3BP1/2 and found that depletion of G3BP1/2 induced less pronounced translation
309 inhibitory effects at 9 and 12 h p.i. in MERS-CoV-Δp4-infected cells (Fig. 7D). Western blot
310 analysis showed that accumulation of structural proteins of MERS-CoV-Δp4 was stronger in
311 cells depleted of TIA-1 or G3BP1/2 than in control siRNA-treated cells (Fig. 7E), whereas
312 depletion of TIA-1 or G3BP1/2 did not affect accumulation of viral mRNAs, mRNA 1, and
313 mRNA 8 (Fig. 7F). These data demonstrated that inhibition of SG accumulation promoted
314 translation of viral and host proteins.

Because SG formation occurs downstream of eIF2α phosphorylation, we anticipated that inhibition of SG formation by depletion of TIA-1 or G3BP1/2 would not affect the status of eIF2α phosphorylation in infected cells. Consistent with this anticipation, depletion of TIA-1 or G3BP1/2 did not alter eIF2α phosphorylation levels in MERS-CoV-Δp4-infected HeLa/CD26 cells and MERS-CoV-WT-infected HeLa/CD26 cells (Figs. 7G and 7H). These data revealed that increased viral gene expression of MERS-CoV-Δp4 in cells depleted TIA-1 or G3BP1/2 was not due to changes in eIF2α phosphorylation.

Taken together, these data were consistent with a notion that SG formation prevented translation by sequestering various factors that are involved in translation to SGs and preventing them to engage translation, leading to inefficient virus replication.

Deletion of 4a gene alone is sufficient for suppression of SG formation in infected cells To establish that 4a accessory protein inhibits SG formation in MERS-CoV infection, we examined SG formation in HeLa/CD26 cells that were infected with MERS-CoV lacking 4a ORF (MERS-CoV-Δ4a) (Fig. 8A). Immunofluorescence analysis using specific antibodies for SG markers, TIA-1, or G3BP, together with MERS-CoV N protein, showed accumulation of SGs in MERS-CoV-Δ4a-infected cells (Fig. 8B and C). There were no notable differences in the quantity of SGs per cell or the number of SG-positive cells between MERS-CoV-Δp4-infected and MERS-CoV-Δ4a-infected cells. As expected, accumulation of 4b protein, but not 4a protein, occurred in MERS-CoV-Δ4a-infected cells (Fig. 9A), demonstrating that 4a accessory protein alone was sufficient for inhibiting SG formation in infected cells. Efficient phosphorylation of PKR and eIF2α occurred in MERS-CoV-Δ4a-infected cells (Fig. 9A), establishing that 4a protein alone was sufficient for inhibition of PKR-mediated eIF2α phosphorylation in infected cells. Pulse

338 radiolabeling experiments showed less efficient translational activities in MERS-CoV-Δ4a-
339 infected cells than in MERS-CoV-WT-infected cells after 9 h p.i. (Fig. 9B), suggesting that a
340 combined effect of SG formation and efficient eIF2α phosphorylation caused strong translational
341 suppression in MERS-CoV-Δ4a-infected cells. There were not substantial differences in the
342 accumulation levels of viral mRNAs between MERS-CoV-Δ4a-infected cells and MERS-CoV-
343 WT-infected cells, except that the former had slightly lower levels of mRNA 4 than the latter
344 (Fig. 9C). Accumulation of viral structural proteins was higher in MERS-CoV-WT-infected cells
345 than in MERS-CoV-Δ4a-infected cells (Fig. 9D), demonstrating that 4a protein inhibited viral
346 translation without affecting viral RNA accumulation. We suspect that inefficient translational
347 activity and lower levels of mRNA 4 accumulation in MERS-CoV-Δ4a-infected cells contributed
348 to the lower level of 4b protein accumulation in MERS-CoV-Δ4a-infected cells than in MERS-
349 CoV-WT-infected cells (Fig. 9A). MERS-CoV-Δ4a replicated less efficiently than MERS-CoV-
350 WT in HeLa/CD26 cells, regardless of the MOI (Fig. 9E). In contrast, both viruses replicated to
351 comparable levels with similar kinetics in Vero cells both at high and low MOIs, except that the
352 titers of MERS-CoV-Δ4a were statistically lower than those of MERS-CoV-WT at 36 h p.i. at an
353 MOI of 3 (Fig. 9F). Taken together, these data supported the notion that due to absence of 4a
354 protein, MERS-CoV-Δ4a induced efficient PKR-mediated eIF2α phosphorylation and SG
355 formation, both of which caused inhibition of viral and host translation, resulting in inefficient
356 virus replication in HeLa/CD26 cells. Overall, MERS-CoV-Δ4a and MERS-CoV-Δp4 showed
357 similar virological properties and induced analogous changes in translational activities and
358 phosphorylation statuses of PKR and eIF2α, strongly suggesting that observed biological
359 differences between MERS-CoV-Δp4 and MERS-CoV-WT in infected HeLa/CD26 cells were
360 primarily due to the absence of 4a protein in MERS-CoV-Δp4-infected cells.

Discussion

SG formation or inhibition has been reported for various viruses, including CoVs (37, 38). TGEV and MHV induce SG or SG-like granules (51, 52) and MERS-CoV did not induce SGs in Vero cells (53), yet the biological roles of SGs or absence of SGs in CoV replication are unknown. The present study demonstrated that replication of MERS-CoV-Δp4 and MERS-CoV-Δ4a, but not MERS-CoV-WT, induced SG formation in HeLa/CD26 cells. MERS-CoV-Δp4 and MERS-CoV-Δ4a replicated less efficiently than MERS-CoV-WT (Figs. 2 and 9) and inhibition of SG formation promoted MERS-CoV-Δp4 replication in this cell line (Fig. 7), demonstrating that SG formation was detrimental for MERS-CoV replication. The less efficient replication of MERS-CoV-Δp4 was at least partly due to attenuation of viral protein synthesis, which was not caused by induction of type I and type III IFNs nor by sequestering viral mRNAs to the SGs. Rather, our data suggested that high levels of PKR-mediated eIF2α phosphorylation and sequestering host factors that are required for translation to the SGs prevented viral translation in MERS-CoV-Δp4 replication. To our knowledge, this is the first report uncovering the biological role of SGs in CoV infection and identifying a CoV protein that suppresses SG accumulation in infected cells.

We observed cell type-dependent SG formation in MERS-CoV-Δp4 infection; SG formation occurred in HeLa/CD26 cells and 293/CD26 cells, but not in Vero cells (Fig. 1). Our data were consistent with a past study reporting the absence of SG formation in Vero cells infected with MERS-CoV and its mutant lacking 4a and 4b ORFs (53). Because translational suppression induced by phosphorylated eIF2α triggers SG formation (27, 28, 30), efficient eIF2α phosphorylation-mediated translational suppression, which occurred in MERS-CoV-Δp4-

384 infected HeLa/CD26 cells but not in MERS-CoV-Δp4-infected Vero cells, most likely
385 contributed to SG formation in HeLa/CD26 cells. PKR expression is low in Vero cells (54) and
386 levels of phosphorylated PKR were similar between MERS-CoV-Δp4-infected Vero cells and
387 MERS-CoV-WT-infected Vero cells (Fig. 3B). In contrast, MERS-CoV-Δp4 replication, but not
388 MERS-CoV-WT replication, induced efficient PKR phosphorylation in HeLa/CD26 cells (Fig.
389 3A). MERS-CoV-Δ4a replication also induced efficient PKR phosphorylation in HeLa/CD26
390 cells (Fig. 9A). These data suggest that low level expression of PKR in Vero cells masked the
391 effects of the 4a protein for inhibiting eIF2α-mediated SG formation in MERS-CoV-Δp4
392 replication. Likewise, replication of a herpes simplex virus type 1 mutant activates PKR and
393 induces eIF2α phosphorylation in HeLa cells, but not in Vero cells (57). In addition to the
394 presence of a genetic defect for IFN production (58, 59), low expression levels of PKR, which
395 was insufficient for PKR-induced eIF2α phosphorylation and SG formation in MERS-CoV-Δp4
396 replication and MERS-CoV-Δ4a replication, might have contributed to efficient replication of
397 various viruses in Vero cells.

398 Translation of viral proteins were less efficient in MERS-CoV-Δp4-infected HeLa/CD26
399 cells than in MERS-CoV-WT-infected HeLa/CD26 cells (Fig. 4D). Likewise, inefficient viral
400 protein synthesis occurred in MERS-CoV-Δ4a replication (Fig. 9B). In contrast, the amount of
401 viral mRNAs were similar in these cells (Figs. 4B, 4C, 9C). As nsp3-nsp16 and N proteins (13,
402 60, 61) drive viral RNA synthesis, it is somewhat puzzling that difference in the translational
403 efficiency of viral proteins did not result in differences in the accumulation of the viral mRNAs.
404 We noted that these three viruses showed similar levels of translational activities (Figs. 3C and
405 9B) and N protein accumulation (Figs. 4D and 9D) at 6 h p.i., implying that they accumulated
406 similar levels of nsp3-nsp16 and N proteins early in infection. If this is the case and if the nsp3-

nsp16 and N proteins, which are synthesized early in infection, primarily determine viral mRNA synthesis efficiency, it would result in similar levels of viral mRNA accumulation in cells infected with these three viruses.

Absence of SG formation in MERS-CoV-Δp4-infected Vero cells led Rabouw *et al*. to suspect that MERS-CoV encodes at least one other stress response antagonist with a mode of action that differs from that of 4a (53). MERS-CoV-Δp4 replication in HeLa/CD26 cells induced SGs in ~100% of infected cells by 12 h p.i., while SGs were detected in very small numbers of MERS-CoV-WT-infected HeLa/CD26 cells (Fig. 1F). Furthermore, MERS-CoV-Δ4a induced SGs in HeLa/CD26 cells (Figs. 8B and 8C). These data suggest that 4a accessory protein is the stress response antagonist that inhibits formation of SGs and that MERS-CoV does not encode another protein(s) that efficiently suppresses SG formation. It should be also noted that the number of SG-positive cells increased according to the progression of MERS-CoV-Δp4 replication (Fig. 1F). Steady SG accumulation during MERS-CoV-Δp4 replication differed from transient induction and disruption of SGs during replication of some viruses (49, 62). These data imply that MERS-CoV does not encode a protein that disrupts pre-existing SGs.

Several past studies reported that SGs serve as a platform for the sensing of non-self RNA by RLRs and that SG formation is important for the innate immunity response during viral infection (31, 35, 36), whereas MERS-CoV-Δp4 infection did not induce accumulation of *IFN-β*, *IFN-λ1*, *OAS*, and *ISG56* mRNAs in HeLa/CD26 cells (Fig. 5). Likewise, Rabouw *et al*. reported the absence of IFNβ production in MERS-CoV-Δp4-infected Huh-7 cells (53). Several possibilities are conceivable for the lack of accumulation of those mRNAs involved in innate immune responses in MERS-CoV-Δp4 infection. One is that poor accumulation of viral mRNAs in the SGs (Fig. 6) prevented recognition of viral mRNAs by RLRs in the SGs. If true, there is a

430 possibility that MERS-CoV alters the cellular environment to actively prevent accumulation of
431 viral mRNAs in SGs. Another possibility is that the SGs could not serve as a platform for
432 sensing of viral mRNAs due to low concentration of RLRs in the SGs. Alternatively, SGs might
433 have served as a sensing platform of viral mRNAs by RLRs, yet another viral protein(s)
434 prevented accumulation of innate immune mRNAs by inhibiting the signaling pathways that
435 induce them, suppressing their transcription/processing or promoting their degradation.

436 Depletion of TIA-1 or G3BP1/2 reduced the number of SGs and promoted viral and host
437 translation and MERS-CoV-Δp4 replication, without affecting levels of eIF2α phosphorylation
438 (Fig. 7G and H). These data strongly suggest that SG formation itself interfered with translation.
439 As viral mRNAs are not confined in the SGs (Fig. 6), we suspect that the confinement of various
440 factors that are required for translation, e.g., translation factors and 40S ribosomes, in the SGs
441 interfered with efficient translation in MERS-CoV-Δp4-infected HeLa/CD26 cells. Although
442 depletion of TIA-1 or G3BP1/2 promoted replication of MERS-CoV-Δp4, it inhibited replication
443 of MERS-CoV-WT (Fig. 7). These data suggested that the inhibition of SG formation by
444 depleting TIA-1 or G3BP1/2 was more pronounced than the effect of TIA-1 and G3BP1/2 for
445 promoting virus replication. Some viruses, e.g., flaviviruses and alphaviruses, inhibit SG
446 accumulation by using certain SG components for viral RNA synthesis (63-65). Accordingly,
447 MERS-CoV may also prevent SG formation to exploit TIA-1 and G3BP1/2 for virus replication.
448 As accumulation of viral mRNAs were similar between MERS-CoV-WT-infected HeLa/CD26
449 cells and MERS-CoV-Δp4-infected HeLa/CD26 cells (Figs. 4A-4C), TIA-1 and G3BP1/2 may
450 promote virus replication at the post-viral transcription step.

451 MERS-CoV accessory proteins encoded from ORF 3 to ORF 5 have major implications
452 for viral replication and pathogenesis in the mouse model (18), while the role of 4a accessory

453 protein in viral pathogenicity is unclear. Unlike Vero cells, many cells in animal hosts likely
454 express PKR, the levels of which are sufficient for eIF2α phosphorylation and inhibition of viral
455 translation; otherwise, cells expressing low levels of PKR would be highly susceptible to virus
456 infection and this would be detrimental for host survival against virus infection. Accordingly, we
457 speculate that MERS-CoV-Δp4 and MERS-CoV-Δ4a induce SGs, which suppress viral
458 translation, in most of the susceptible cells/organs in infected animals. Testing pathogenesis of
459 MERS-CoV-Δp4 and MERS-CoV-Δ4a in the mouse model would provide a clue as to the role of
460 SGs in MERS-CoV pathogenesis.
461

462 **Materials and Methods**

463 **Cells.** Vero cells were maintained in Dulbecco modified Eagle medium supplemented with
464 10% fetal bovine serum. HeLa/CD26 cells and 293/CD26 cells were generated by transfecting
465 pCAGGS-CD26-BlasticidinR, which expresses the blasticidin resistance gene and human CD26,
466 into HeLa cells and 293 cells (ATCC), respectively, and incubating the transfected cells in
467 selection medium containing blasticidin (12 μg/ml) for two weeks. Stable expression of human
468 CD26 in 293/CD26 and HeLa/CD26 cells were confirmed by Western blot analysis with anti-
469 human DPP4 antibody (R&D systems).
470

471 **Viruses.** MERS-CoV-WT, MERS-CoV-Δp4 lacking ORFs 4a and 4b, and MERS-CoV-Δ4a
472 lacking ORF 4a were rescued by using a reverse genetics system of MERS-CoV (55). Briefly, a
473 recombinant PCR procedure was used to delete both ORFs 4a and 4b or only ORF 4a in
474 fragment F of the MERS-CoV reverse genetics system (55). After assembly of the MERS-CoV
475 full-length cDNA by ligating fragments A through F, we synthesized the full-length RNA

476 transcripts, and rescued the recombinant viruses according to established protocols, as described
477 previously (55). MERS-CoV-Δp4 and MERS-CoV-Δ4a had a deletion at from nt 25,852 to
478 26,833 and from nt 25,852 to 26,181, respectively, in the MERS-CoV genomic RNA (GenBank
479 accession number: JX869059.2). We passaged the rescued viruses once in Vero cells, confirmed
480 the presence of the expected mutation in MERS-CoV-Δp4 and MERS-CoV-Δ4a and absence of
481 the mutation at the corresponding region in MERS-CoV-WT, and used for experiments. All
482 experiments with infectious MERS-CoV were performed in an approved biosafety level 3
483 laboratory at The University of Texas Medical Branch at Galveston. Sendai virus (SeV; Cantell
484 strain), obtained from Charles River Laboratory (Wilmington, MA), was used to infect cells at
485 400 hemagglutination units/ml.
486
487 **Immunofluorescence staining and CHX treatment.** Cells were fixed overnight with 4%
488 paraformaldehyde, and permeabilized for 15 min with 0.1% Triton X-100 in phosphate-buffered
489 saline (PBS). After blocking with 1% bovine serum albumin in PBS for 1 h, the cells were
490 incubated with primary antibodies (anti-MERS-CoV N protein antibody and goat anti-TIA1
491 antibody [Santa Cruz], mouse anti-G3BP antibody [BD Biosciences], or mouse anti-eIF4AI/II
492 antibody [Santa Cruz]) overnight at 4˚C, washed, and incubated for 1 h at room temperature with
493 Alexafluor conjugated secondary antibodies (Thermo Fisher Scientific). Anti-MERS-CoV N
494 protein antibody was generated by immunizing rabbits with synthetic peptide
495 (NDITNTNLSRGRGRNPKPR). Fluorescence was visualized by using a ZEISS Axioplan 2
496 imaging. For CHX treatment, HeLa/CD26 cells were infected with virus at an MOI of 3. At 8 h
497 p.i., medium was replaced with growth medium containing 100 µg/ml CHX (Sigma) dissolved in
498 DMSO. An equal volume of DMSO was added to the control medium. At 9 h p.i., cells were

fixed and processed for immunofluorescence staining for anti-MERS-CoV N protein antibody and TIA-1 antibody, as described above.

Fluorescent *in situ* hybridization. MERS-CoV mRNAs were detected by using a DIG-labeled riboprobe binding to nt 29,084 to 29,608 of the MERS-CoV genomic RNA. The probe was denatured at 100˚C for 10 min, diluted 1:1 in hybridization buffer (2% SSC, 10% dextran sulfate), and hybridized to the cells at 45˚C for 18 h. After two washes using wash buffer I (50% formamide, 0.1% SDS and 0.1 % SSC) and one subsequent wash with wash buffer II (50% formamide and 0.2% SSC), cells were incubated with anti-digoxigenin-fluorescein (Sigma-Aldrich) and anti-eIF4AI/II antibodies overnight at 4˚C. Then, the cells were washed in wash buffer III (8% formamid and 2% SSC), and incubated for 1 h at room temperature with Alexafluor conjugated secondary antibodies (Thermo Fisher Scientific). Images were captured by a Zeiss Axiophot 2 fluorescence microscopy and processed with ImageJ software (http://rsbweb.nih.gov/ij/).

Virus growth in Vero and HeLa/CD26 cells. Monolayer cultures of Vero cells or HeLa/CD26 cells were infected with MERS-CoV-WT, MERS-CoV-Δp4, or MERS-CoV-Δ4a at an MOI of 0.01 or 3 for 1 h at 37˚C. After virus adsorption, cells were washed twice with PBS and incubated with the appropriate medium. Viruses in the culture supernatants were harvested at different times p.i. The infectious virus titers were determined by plaque assay by using Vero cells and expressed in plaque forming unit (PFU) per ml.

521 **Western blot analysis.** Confluent cells were infected with MERS-CoV-WT, MERS-CoV-Δp4,
522 or MERS-CoV-Δ4a at an MOI of 3. At different times p.i., cells were lysed in sodium sulfate-
523 polyacrylamide gel electrophoresis (SDS-PAGE) sample buffer. Anti-PKR (Abcam) antibody,
524 anti-phospho-PKR antibody (Abcam), anti-eIF2α antibody (Cell Signaling Technology), anti-
525 phosphorylated eIF2α antibody (Cell Signaling Technology), anti-α-tubulin antibody
526 (CALBIOCHEM), anti-MERS-CoV N protein antibody, or the following antibodies for MERS-
527 CoV proteins were used as primary antibodies: anti-MERS-CoV S protein antibody, anti-MERS-
528 CoV M protein antibody, anti-MERS-CoV 4a protein antibody and anti-MERS-CoV 4b protein
529 antibody were generated by immunizing rabbits with the synthetic peptides
530 DDRTEVPQLVNANQYSPCVSIVC, CDYDRLPNEVTVAK, QRIAWLLHKDGGIPD, and
531 RKARKRSHSPTKKLRYVKRR, respectively. The secondary antibodies consisted of goat anti-
532 mouse immunoglobulin G–horseradish peroxidase and goat anti-rabbit immunoglobulin G–
533 horseradish peroxidase (Santa Cruz).
534
535 **Metabolic radiolabeling of intracellular proteins in virus-infected cells.** Vero or HeLa/CD26
536 cells were mock-infected or infected with MERS-CoV-WT, MERS-CoV-Δp4, or MERS-CoV-
537 Δ4a at an MOI of 3. Cells were radiolabeled with 100 μCi of Tran^{35}S-label/ml (PerkinElmer) for
538 1 h at different times p.i. The cell extracts were prepared by lysing the cells in SDS-PAGE
539 sample buffer. Cell lysates were subjected to SDS-PAGE analysis, followed by autoradiography
540 and colloid Coomassie brilliant blue staining.
541
542 **Total RNA extraction and qRT-PCR** Total cellular RNAs were extracted from cells by using
543 TRIzol LS reagent (Invitrogen) and Direct-zol RNA MiniPrep (Zymo Research), following

544 instruction manuals. cDNAs were synthesized using SuperScript III reverse transcriptase
545 (Invitrogen) and random primers (Invitrogen). To specifically detect MERS-CoV mRNAs,
546 MERS-CoV gene specific primers, 5′-TTTTTTTTCTAATCAGTGTTAACATCAATCATTGG-
547 3′, were used for cDNA synthesis. qRT-PCR was performed using a Bio-Rad CFX96 real-time
548 PCR apparatus and SYBR green Master mix (Bio-Rad). PCR conditions were as follows:
549 preincubation at 95°C for 30 s and amplification with 40 cycles of 95°C for 15 s and 60°C for 20
550 s. The purity of the amplified PCR products was confirmed by the dissociation melting curves
551 obtained after each reaction. The primers used for human *IFN-β* mRNA were 5′-
552 AAGGCCAAGGAGTACAGTC-3′ (forward) and 5′-ATCTTCAGTTTVGGAGGTAA-3′
553 (reverse); the primers for *IFN-λ* mRNA were 5′-CGCCTTGGAAGAGTCACTCA-3′ (forward)
554 and 5′-GAAGCCTCAGGTCCCAATTC-3′ (reverse); the primers for *OAS* mRNA were 5′-
555 GCCCTGGGTCAGTTGACTGG-3′ (forward) and 5′-TGAAGCAGGTGGAGAACTCGC-3′
556 (reverse); the primers for *ISG56* mRNA were 5′-CAGCAACCATGAGTACAAAT-3′ (forward)
557 and 5′-AAGTGACATCTCAATTGCTC-3′ (reverse); the primers for 18S rRNA were 5′-
558 CCGGTACAGTGAAACTGCGAATG-3′ (forward) and 5′-
559 GTTATCCAAGTAGGAGAGGAGCGAG-3′ (reverse); the primers for MERS-CoV mRNA 1
560 were 5′-AATACACGGTTTCGTCCGGTG-3′ (forward) and 5′-
561 ACCACAGAGTGGCACAGTTAG-3′ (reverse); the primers for MERS-CoV mRNA 8 were 5′-
562 CTCGTTCTCTTGCAGAACTTTG-3′ (forward) and 5′-TGCCCAGGTGGAAAGGT-3′
563 (reverse). The relative expression level of each gene mRNA was normalized to 18S rRNA levels.
564 All of the assays were performed in triplicate, and the results are expressed as means ± the
565 standard deviations.
566

Northern blot analysis. Total cellular RNAs were extracted from mock-infected cells or infected cells as described above. A DIG-labeled riboprobe, corresponding to nt 29,084 to 29,608 of the MERS-CoV genomic RNA, was used to detect MERS-CoV mRNAs as described previously (56).

siRNA treatment. HeLa/CD26 cells were transfected with the indicated siRNAs using RNAiMAX according to the manufacturer's protocol (Invitrogen). Non-targeting siRNA (Dharmacon) and siRNA targeting G3BP1 (Thermo Fisher Scientific), G3BP2 (Thermo Fisher Scientific), or TIA-1 (Dharmacon) were used. At 24 h posttransfection, cells were either mock-infected or infected with MERS-CoV-WT or MERS-CoV-Δp4 at an MOI of 3.

Statistical Analysis Two-tailed Student's t test was conducted to determine statistical significance. Statistical significance was defined as a *P* value of <0.05.

Acknowledgements

We thank Ralph Baric for kindly providing us the MERS-CoV reverse genetics system. This study was supported by Public Health Service grants AI99107 and AI114657 from the National Institutes of Health and a grant from the Institute for Human Infections and Immunity at The University of Texas Medical Branch. K. Nakagawa was supported by the James W. McLaughlin fellowship fund.

References

1. Zaki AM, van Boheemen S, Bestebroer TM, Osterhaus AD, Fouchier RA. 2012. Isolation of a novel coronavirus from a man with pneumonia in Saudi Arabia. N Engl J Med 367:1814-20.

591 2. Alagaili AN, Briese T, Mishra N, Kapoor V, Sameroff SC, Burbelo PD, de Wit E, Munster VJ,
592 Hensley LE, Zalmout IS, Kapoor A, Epstein JH, Karesh WB, Daszak P, Mohammed OB, Lipkin WI.
593 2014. Middle East respiratory syndrome coronavirus infection in dromedary camels in Saudi
594 Arabia. MBio 5:e00884-14.
595 3. Wernery U, Lau SK, Woo PC. 2017. Middle East respiratory syndrome (MERS) coronavirus and
596 dromedaries. Vet J 220:75-79.
597 4. Chu DK, Poon LL, Gomaa MM, Shehata MM, Perera RA, Abu Zeid D, El Rifay AS, Siu LY, Guan Y,
598 Webby RJ, Ali MA, Peiris M, Kayali G. 2014. MERS coronaviruses in dromedary camels, Egypt.
599 Emerg Infect Dis 20:1049-53.
600 5. Drosten C, Kellam P, Memish ZA. 2014. Evidence for camel-to-human transmission of MERS
601 coronavirus. N Engl J Med 371:1359-60.
602 6. Drosten C, Gunther S, Preiser W, van der Werf S, Brodt HR, Becker S, Rabenau H, Panning M,
603 Kolesnikova L, Fouchier RA, Berger A, Burguiere AM, Cinatl J, Eickmann M, Escriou N, Grywna K,
604 Kramme S, Manuguerra JC, Muller S, Rickerts V, Sturmer M, Vieth S, Klenk HD, Osterhaus AD,
605 Schmitz H, Doerr HW. 2003. Identification of a novel coronavirus in patients with severe acute
606 respiratory syndrome. N Engl J Med 348:1967-76.
607 7. Lee HJ, Shieh CK, Gorbalenya AE, Koonin EV, La Monica N, Tuler J, Bagdzhadzhyan A, Lai MM.
608 1991. The complete sequence (22 kilobases) of murine coronavirus gene 1 encoding the
609 putative proteases and RNA polymerase. Virology 180:567-82.
610 8. Lomniczi B. 1977. Biological properties of avian coronavirus RNA. J Gen Virol 36:531-3.
611 9. Lomniczi B, Kennedy I. 1977. Genome of infectious bronchitis virus. J Virol 24:99-107.
612 10. Raj VS, Mou H, Smits SL, Dekkers DH, Muller MA, Dijkman R, Muth D, Demmers JA, Zaki A,
613 Fouchier RA, Thiel V, Drosten C, Rottier PJ, Osterhaus AD, Bosch BJ, Haagmans BL. 2013.
614 Dipeptidyl peptidase 4 is a functional receptor for the emerging human coronavirus-EMC.
615 Nature 495:251-4.
616 11. Hurst-Hess KR, Kuo L, Masters PS. 2015. Dissection of amino-terminal functional domains of
617 murine coronavirus nonstructural protein 3. J Virol 89:6033-47.
618 12. Graham RL, Sims AC, Brockway SM, Baric RS, Denison MR. 2005. The nsp2 replicase proteins of
619 murine hepatitis virus and severe acute respiratory syndrome coronavirus are dispensable for
620 viral replication. J Virol 79:13399-411.
621 13. Neuman BW, Chamberlain P, Bowden F, Joseph J. 2014. Atlas of coronavirus replicase structure.
622 Virus Res 194:49-66.
623 14. Lai MM, Baric RS, Brayton PR, Stohlman SA. 1984. Characterization of leader RNA sequences on
624 the virion and mRNAs of mouse hepatitis virus, a cytoplasmic RNA virus. Proc Natl Acad Sci U S A
625 81:3626-30.
626 15. Lai MM, Patton CD, Baric RS, Stohlman SA. 1983. Presence of leader sequences in the mRNA of
627 mouse hepatitis virus. J Virol 46:1027-33.
628 16. Leibowitz JL, Wilhelmsen KC, Bond CW. 1981. The virus-specific intracellular RNA species of two
629 murine coronaviruses: MHV-a59 and MHV-JHM. Virology 114:39-51.
630 17. Spaan WJ, Rottier PJ, Horzinek MC, van der Zeijst BA. 1982. Sequence relationships between the
631 genome and the intracellular RNA species 1, 3, 6, and 7 of mouse hepatitis virus strain A59. J
632 Virol 42:432-9.
633 18. Menachery VD, Mitchell HD, Cockrell AS, Gralinski LE, Yount BL, Jr., Graham RL, McAnarney ET,
634 Douglas MG, Scobey T, Beall A, Dinnon K, 3rd, Kocher JF, Hale AE, Stratton KG, Waters KM, Baric
635 RS. 2017. MERS-CoV Accessory ORFs Play Key Role for Infection and Pathogenesis. MBio 8.
636 19. Thornbrough JM, Jha BK, Yount B, Goldstein SA, Li Y, Elliott R, Sims AC, Baric RS, Silverman RH,
637 Weiss SR. 2016. Middle East Respiratory Syndrome Coronavirus NS4b Protein Inhibits Host
638 RNase L Activation. MBio 7:e00258.

639 20. Matthews KL, Coleman CM, van der Meer Y, Snijder EJ, Frieman MB. 2014. The ORF4b-encoded
640 accessory proteins of Middle East respiratory syndrome coronavirus and two related bat
641 coronaviruses localize to the nucleus and inhibit innate immune signalling. J Gen Virol 95:874-82.
642 21. Niemeyer D, Zillinger T, Muth D, Zielecki F, Horvath G, Suliman T, Barchet W, Weber F, Drosten C,
643 Muller MA. 2013. Middle East respiratory syndrome coronavirus accessory protein 4a is a type I
644 interferon antagonist. J Virol 87:12489-95.
645 22. Canton J, Fehr AR, Fernandez-Delgado R, Gutierrez-Alvarez FJ, Sanchez-Aparicio MT, Garcia-
646 Sastre A, Perlman S, Enjuanes L, Sola I. 2018. MERS-CoV 4b protein interferes with the NF-
647 kappaB-dependent innate immune response during infection. PLoS Pathog 14:e1006838.
648 23. Holcik M, Sonenberg N. 2005. Translational control in stress and apoptosis. Nat Rev Mol Cell Biol
649 6:318-27.
650 24. Garcia MA, Meurs EF, Esteban M. 2007. The dsRNA protein kinase PKR: virus and cell control.
651 Biochimie 89:799-811.
652 25. Farrell PJ, Balkow K, Hunt T, Jackson RJ, Trachsel H. 1977. Phosphorylation of initiation factor
653 eIF-2 and the control of reticulocyte protein synthesis. Cell 11:187-200.
654 26. Wek RC, Jiang HY, Anthony TG. 2006. Coping with stress: eIF2 kinases and translational control.
655 Biochem Soc Trans 34:7-11.
656 27. Anderson P, Kedersha N. 2008. Stress granules: the Tao of RNA triage. Trends Biochem Sci
657 33:141-50.
658 28. Anderson P, Kedersha N. 2009. Stress granules. Curr Biol 19:R397-8.
659 29. Kedersha N, Anderson P. 2009. Regulation of translation by stress granules and processing
660 bodies. Prog Mol Biol Transl Sci 90:155-85.
661 30. Kedersha NL, Gupta M, Li W, Miller I, Anderson P. 1999. RNA-binding proteins TIA-1 and TIAR
662 link the phosphorylation of eIF-2 alpha to the assembly of mammalian stress granules. J Cell Biol
663 147:1431-42.
664 31. Onomoto K, Jogi M, Yoo JS, Narita R, Morimoto S, Takemura A, Sambhara S, Kawaguchi A, Osari
665 S, Nagata K, Matsumiya T, Namiki H, Yoneyama M, Fujita T. 2012. Critical role of an antiviral
666 stress granule containing RIG-I and PKR in viral detection and innate immunity. PLoS One
667 7:e43031.
668 32. Reineke LC, Lloyd RE. 2015. The stress granule protein G3BP1 recruits protein kinase R to
669 promote multiple innate immune antiviral responses. J Virol 89:2575-89.
670 33. Langereis MA, Feng Q, van Kuppeveld FJ. 2013. MDA5 localizes to stress granules, but this
671 localization is not required for the induction of type I interferon. J Virol 87:6314-25.
672 34. Onomoto K, Yoneyama M, Fung G, Kato H, Fujita T. 2014. Antiviral innate immunity and stress
673 granule responses. Trends Immunol 35:420-8.
674 35. Okonski KM, Samuel CE. 2013. Stress granule formation induced by measles virus is protein
675 kinase PKR dependent and impaired by RNA adenosine deaminase ADAR1. J Virol 87:756-66.
676 36. Ng CS, Jogi M, Yoo JS, Onomoto K, Koike S, Iwasaki T, Yoneyama M, Kato H, Fujita T. 2013.
677 Encephalomyocarditis virus disrupts stress granules, the critical platform for triggering antiviral
678 innate immune responses. J Virol 87:9511-22.
679 37. White JP, Lloyd RE. 2012. Regulation of stress granules in virus systems. Trends Microbiol
680 20:175-83.
681 38. Poblete-Duran N, Prades-Perez Y, Vera-Otarola J, Soto-Rifo R, Valiente-Echeverria F. 2016. Who
682 Regulates Whom? An Overview of RNA Granules and Viral Infections. Viruses 8.
683 39. Khaperskyy DA, Hatchette TF, McCormick C. 2012. Influenza A virus inhibits cytoplasmic stress
684 granule formation. FASEB J 26:1629-39.

685 40. Sciortino MT, Parisi T, Siracusano G, Mastino A, Taddeo B, Roizman B. 2013. The virion host
686 shutoff RNase plays a key role in blocking the activation of protein kinase R in cells infected with
687 herpes simplex virus 1. J Virol 87:3271-6.
688 41. Cassady KA, Gross M. 2002. The herpes simplex virus type 1 U(S)11 protein interacts with
689 protein kinase R in infected cells and requires a 30-amino-acid sequence adjacent to a kinase
690 substrate domain. J Virol 76:2029-35.
691 42. He B, Gross M, Roizman B. 1997. The gamma(1)34.5 protein of herpes simplex virus 1 complexes
692 with protein phosphatase 1alpha to dephosphorylate the alpha subunit of the eukaryotic
693 translation initiation factor 2 and preclude the shutoff of protein synthesis by double-stranded
694 RNA-activated protein kinase. Proc Natl Acad Sci U S A 94:843-8.
695 43. Mulvey M, Arias C, Mohr I. 2007. Maintenance of endoplasmic reticulum (ER) homeostasis in
696 herpes simplex virus type 1-infected cells through the association of a viral glycoprotein with
697 PERK, a cellular ER stress sensor. J Virol 81:3377-90.
698 44. Simpson-Holley M, Kedersha N, Dower K, Rubins KH, Anderson P, Hensley LE, Connor JH. 2011.
699 Formation of antiviral cytoplasmic granules during orthopoxvirus infection. J Virol 85:1581-93.
700 45. White JP, Cardenas AM, Marissen WE, Lloyd RE. 2007. Inhibition of cytoplasmic mRNA stress
701 granule formation by a viral proteinase. Cell Host Microbe 2:295-305.
702 46. Sun Y, Dong L, Yu S, Wang X, Zheng H, Zhang P, Meng C, Zhan Y, Tan L, Song C, Qiu X, Wang G,
703 Liao Y, Ding C. 2017. Newcastle disease virus induces stable formation of bona fide stress
704 granules to facilitate viral replication through manipulating host protein translation. FASEB J
705 31:1337-1353.
706 47. Heinrich BS, Cureton DK, Rahmeh AA, Whelan SP. 2010. Protein expression redirects vesicular
707 stomatitis virus RNA synthesis to cytoplasmic inclusions. PLoS Pathog 6:e1000958.
708 48. Dinh PX, Beura LK, Das PB, Panda D, Das A, Pattnaik AK. 2013. Induction of stress granule-like
709 structures in vesicular stomatitis virus-infected cells. J Virol 87:372-83.
710 49. Garaigorta U, Heim MH, Boyd B, Wieland S, Chisari FV. 2012. Hepatitis C virus (HCV) induces
711 formation of stress granules whose proteins regulate HCV RNA replication and virus assembly
712 and egress. J Virol 86:11043-56.
713 50. Ruggieri A, Dazert E, Metz P, Hofmann S, Bergeest JP, Mazur J, Bankhead P, Hiet MS, Kallis S,
714 Alvisi G, Samuel CE, Lohmann V, Kaderali L, Rohr K, Frese M, Stoecklin G, Bartenschlager R. 2012.
715 Dynamic oscillation of translation and stress granule formation mark the cellular response to
716 virus infection. Cell Host Microbe 12:71-85.
717 51. Sola I, Galan C, Mateos-Gomez PA, Palacio L, Zuniga S, Cruz JL, Almazan F, Enjuanes L. 2011. The
718 polypyrimidine tract-binding protein affects coronavirus RNA accumulation levels and relocalizes
719 viral RNAs to novel cytoplasmic domains different from replication-transcription sites. J Virol
720 85:5136-49.
721 52. Raaben M, Groot Koerkamp MJ, Rottier PJ, de Haan CA. 2007. Mouse hepatitis coronavirus
722 replication induces host translational shutoff and mRNA decay, with concomitant formation of
723 stress granules and processing bodies. Cell Microbiol 9:2218-29.
724 53. Rabouw HH, Langereis MA, Knaap RC, Dalebout TJ, Canton J, Sola I, Enjuanes L, Bredenbeek PJ,
725 Kikkert M, de Groot RJ, van Kuppeveld FJ. 2016. Middle East Respiratory Coronavirus Accessory
726 Protein 4a Inhibits PKR-Mediated Antiviral Stress Responses. PLoS Pathog 12:e1005982.
727 54. Park SH, Choi J, Kang JI, Choi SY, Hwang SB, Kim JP, Ahn BY. 2006. Attenuated expression of
728 interferon-induced protein kinase PKR in a simian cell devoid of type I interferons. Mol Cells
729 21:21-8.
730 55. Scobey T, Yount BL, Sims AC, Donaldson EF, Agnihothram SS, Menachery VD, Graham RL,
731 Swanstrom J, Bove PF, Kim JD, Grego S, Randell SH, Baric RS. 2013. Reverse genetics with a full-

length infectious cDNA of the Middle East respiratory syndrome coronavirus. Proc Natl Acad Sci U S A 110:16157-62.

56. Lokugamage KG, Narayanan K, Nakagawa K, Terasaki K, Ramirez SI, Tseng CT, Makino S. 2015. Middle East Respiratory Syndrome Coronavirus nsp1 Inhibits Host Gene Expression by Selectively Targeting mRNAs Transcribed in the Nucleus while Sparing mRNAs of Cytoplasmic Origin. J Virol 89:10970-81.

57. Dauber B, Poon D, Dos Santos T, Duguay BA, Mehta N, Saffran HA, Smiley JR. 2016. The Herpes Simplex Virus Virion Host Shutoff Protein Enhances Translation of Viral True Late mRNAs Independently of Suppressing Protein Kinase R and Stress Granule Formation. J Virol 90:6049-57.

58. Emeny JM, Morgan MJ. 1979. Regulation of the interferon system: evidence that Vero cells have a genetic defect in interferon production. J Gen Virol 43:247-52.

59. Wathelet MG, Berr PM, Huez GA. 1992. Regulation of gene expression by cytokines and virus in human cells lacking the type-I interferon locus. Eur J Biochem 206:901-10.

60. Baric RS, Nelson GW, Fleming JO, Deans RJ, Keck JG, Casteel N, Stohlman SA. 1988. Interactions between coronavirus nucleocapsid protein and viral RNAs: implications for viral transcription. J Virol 62:4280-7.

61. Compton SR, Rogers DB, Holmes KV, Fertsch D, Remenick J, McGowan JJ. 1987. In vitro replication of mouse hepatitis virus strain A59. J Virol 61:1814-20.

62. Panas MD, Varjak M, Lulla A, Eng KE, Merits A, Karlsson Hedestam GB, McInerney GM. 2012. Sequestration of G3BP coupled with efficient translation inhibits stress granules in Semliki Forest virus infection. Mol Biol Cell 23:4701-12.

63. Emara MM, Liu H, Davis WG, Brinton MA. 2008. Mutation of mapped TIA-1/TIAR binding sites in the 3' terminal stem-loop of West Nile virus minus-strand RNA in an infectious clone negatively affects genomic RNA amplification. J Virol 82:10657-70.

64. Li W, Li Y, Kedersha N, Anderson P, Emara M, Swiderek KM, Moreno GT, Brinton MA. 2002. Cell proteins TIA-1 and TIAR interact with the 3' stem-loop of the West Nile virus complementary minus-strand RNA and facilitate virus replication. J Virol 76:11989-2000.

65. Scholte FE, Tas A, Albulescu IC, Zusinaite E, Merits A, Snijder EJ, van Hemert MJ. 2015. Stress granule components G3BP1 and G3BP2 play a proviral role early in Chikungunya virus replication. J Virol 89:4457-69.

Figure Legends

Fig 1. Induction of SGs in MERS-CoV-Δp4-infected cells (A) Schematic diagrams of genomes of MERS-CoV-WT (WT) and MERS-CoV-Δp4 (Δp4). The 5' and 3' untranslated regions (bars) and viral open reading frames (boxes) are not drawn according to their lengths. (B-D) HeLa/CD26 cells were infected with MERS-CoV-WT or MERS-CoV-Δp4 at an MOI of 3. At 9 h p.i., the infected cells were fixed with 4% formaldehyde and stained for TIA-1 (B), G3BP (C), or eIF4A (D) shown in green, together with MERS-CoV N protein shown in red. Right panels show enlarged images of the regions shown in white boxes in the merged image panels.

(E) HeLa/CD26 cells were infected with MERS-CoV-Δp4 at an MOI of 3. At 8 h p.i., the infected cells were treated with 100 μg/ml of CHX or DMSO for 1 h. After fixing, cells were stained for TIA-1 (green) and N protein (red). (F) HeLa/CD26 cells (left panel) or Vero cells (right panel) were infected with MERS-CoV-WT or MERS-CoV-Δp4 at an MOI of 3. At indicated times p.i., cells were fixed, and stained for TIA-1 and MERS-CoV N protein. Among N protein-positive cells, those carrying at least a single TIA-1-postive granule were counted as SG-positive, while SG-negative calls lacked any TIA-1-postive granules. The percentage of SG-positive cells was calculated by counting the number of SG-positive cells out of 25-34 N protein-positive cells/field. A total of 20 fields were counted for each sample. Each bar represents the mean (±standard deviation). (G, H) Vero cells (G) or 293/CD26 cells (H) were mock-infected (Mock) or infected with MERS-CoV-WT (WT) or MERS-CoV-Δp4 (Δp4) at an MOI of 3. At 24 h p.i., the infected cells were fixed with 4% formaldehyde and were stained for G3BP (green), together with MERS-CoV N protein (red).

Fig 2. Growth kinetics of MERS-CoV-WT and MERS-CoV-Δp4 in HeLa/CD26 and Vero cells HeLa/CD26 (A) or Vero cells (B) were infected with MERS-CoV-WT (WT) or MERS-CoV-Δp4 (Δp4) at an MOI of 0.01 (left panels) or 3 (right panels). Culture supernatants were collected at the indicated times p.i., and virus titers were determined by plaque assay. Each dot represents mean virus titers (±standard deviation) from three wells. Asterisks represent statically significant differences in virus titers ($P<0.05$).

Fig 3. Phosphorylation statuses of PKR and eIF2α and efficiencies of host and viral protein synthesis in infected cells HeLa/CD26 cells or Vero cells were either mock-infected (Mock) or

794 infected with MERS-CoV-WT (WT) or MERS-CoV-Δp4 (Δp4) at an MOI of 3. (A and B)
795 Whole cell lysates were prepared at 9 h p.i. for HeLa/CD26 cells (A) and 24 h p.i. for Vero cells
796 (B) and subjected to Western blot analysis to detect PKR, phosphorylated PKR (p-PKR), eIF2α,
797 phosphorylated eIF2α (p-eIF2α), MERS-CoV 4a protein, MERS-CoV 4b protein, and tubulin.
798 HeLa/CD26 cells (C) or Vero cells (D) were radiolabeled for 1 h with 100 μCi of Tran^{35}S-label,
799 and cell lysates were prepared at the indicated times p.i. Cell lysates were subjected to SDS-
800 PAGE analysis, followed by autoradiography (top panels) and colloid Coomassie blue staining
801 (bottom panels). Arrows, virus-specific proteins.
802
803 **Fig 4. Accumulations of viral mRNAs and proteins in infected HeLa/CD26 cells**
804 HeLa/CD26 cells were mock-infected (Mock) or infected with MERS-CoV-WT (WT) or MERS-
805 CoV-Δp4 (Δp4) at an MOI of 3. At indicated times p.i., total intracellular RNAs and proteins
806 were prepared. (A) Northern blot analysis of viral mRNAs using a riboprobe that binds to all
807 viral mRNAs. Numbers 1-8 represent viral mRNA species. The 28S and 18S rRNAs were
808 detected by ethidium bromide staining (rRNA). Amounts of mRNA 1 (B) and subgenomic
809 mRNA 8 (C) were quantified by qRT-PCR. Expression levels of mRNAs were normalized to
810 levels of 18S rRNA. Each bar represents the mean (±standard deviation) of three independent
811 samples. ns, not significant (P>0.05). (D) Western blot analysis of intracellular accumulation of
812 MERS-CoV S, M, N proteins and tubulin.
813
814 **Fig 5. Expression of host mRNAs involved in innate immune responses in infected**
815 **HeLa/CD26 cells** HeLa/CD26 cells were mock-infected (Mock) or infected with MERS-CoV-
816 WT (WT) or MERS-CoV-Δp4 (Δp4) at an MOI of 3. SeV was used as a positive control. Total

817 intracellular RNAs were extracted at the indicated times p.i., and the amounts of endogenous
818 *IFN-β* (A), *IFN-λ* (B), *OAS* (C), *and ISG56* (D) mRNAs were determined by qRT-PCR analysis.
819 Expression levels of the genes were normalized to levels of 18S rRNA. Each bar represents the
820 mean (±standard deviation) from three independent samples. ns, not significant (P>0.05).
821
822 **Fig 6. Subcellular localization of viral mRNAs and a SG marker, eIF4A, in MERS-CoV-**
823 **Δp4-infected cells** HeLa/CD26 cells were mock-infected (top panels) or infected with MERS-
824 CoV-WT (middle panels) or MERS-CoV-Δp4 (bottom panels) at an MOI of 3. At 9 h p.i., viral
825 mRNAs were detected by riboprobe binding to all viral mRNAs (green) and SGs were detected
826 by anti-eIF4A antibody (red). Samples were subjected to fluorescent microscopic examination.
827
828 **Fig 7. SG formation interfered with efficient MERS-CoV replication** HeLa/CD26 cells
829 were transfected with control siRNA (siCont) or siRNA targeting TIA-1 (siTIA-1) or G3BP1/2
830 (siG3BP1/2). (A) At 24 h siRNA posttransfection, cells were infected with MERS-CoV-Δp4 at
831 an MOI of 3. At 9 h p.i., the cells were fixed and stained for G3BP or TIA-1, together with N
832 protein. The numbers of SGs in each N protein-positive cells were counted and average numbers
833 of SGs per cell were calculated. Each bar represents the mean (±standard deviation) for 20 cells
834 infected with MERS-CoV-Δp4. Whole cell lysates were prepared at 24 h posttransfection, and
835 subjected to Western blot analysis to detect TIA-1, G3BP1, G3BP2, or tubulin. (B) At 24 h
836 siRNA posttransfection, cells were infected with MERS-CoV-WT or MERS-CoV-Δp4 at an
837 MOI of 3. The titers of released viruses at the indicated times p.i. were determined by plaque
838 assay. Filled boxes represent virus titers in siCont-transfected cells, while empty boxes represent
839 virus titers insiTIA-1-transfected cells or siG3BP1/2-transfected cells. Each box represents the

840 mean (±standard deviation) for three wells. Asterisks represent statistically significant
841 differences (P<0.05). (C and D) After 24 h siRNA transfection, cells were mock-infected (Mock)
842 or infected with MERS-CoV-WT (WT) or MERS-CoV-Δp4 (Δp4) at an MOI of 3. These cells
843 were radiolabeled for 1 h with 100 μCi of Tran^{35}S-label, and cell lysates were prepared at the
844 indicated times p.i. Cell lysates were subjected to SDS-PAGE analysis, followed by
845 autoradiography (left panels) and colloid Coomassie blue staining (right panels). (E and F) After
846 24 h siRNA transfection, cells were infected with MERS-CoV-Δp4 at an MOI of 3, and total cell
847 lysates and RNAs were prepared at 9 h p.i. Western blot analysis of viral S protein, M protein, N
848 proteins, and tubulin (E). Amounts of mRNA 1 and subgenomic mRNA 8 were quantified by
849 qRT-PCR (F). Expression levels of mRNAs were normalized to levels of 18S rRNA. Each bar
850 represents the mean (±standard deviation) of three independent samples. ns, not significant
851 (P>0.05). (G and H) After 24 h siRNA transfection, cells were mock-infected (Mock) or infected
852 with MERS-CoV-WT (WT) or MERS-CoV-Δp4 (Δp4) at an MOI of 3. Cell lysate were
853 prepared at 9 h p.i., and subjected to Western blot analysis to detect eIF2α and phosphorylated
854 eIF2α (p-eIF2α).
855
856 **Fig 8. MERS-CoV 4a accessory protein alone is sufficient for inhibiting SG formation in**
857 **infected cells** (A) Schematic diagrams of genomes of MERS-CoV-WT (WT) and MERS-CoV-
858 Δ4a (Δ4a). Boxes represent open reading frames derived from MERS-CoV-WT. The 5' and 3'
859 untranslated regions (bars) and viral open reading frames (boxes) are not drawn according to
860 their lengths. (B and C) HeLa/CD26 cells were infected with MERS-CoV-WT or MERS-CoV-
861 Δ4a at an MOI of 3. At 9 h p.i., the infected cells were fixed and stained for TIA-1 or G3BP
862 (green), together with MERS-CoV N protein (red).

Fig. 9. Characterization of MERS-CoV-Δ4a replication in HeLa/CD26 cells HeLa/CD26 cells were either mock-infected (Mock) or infected with MERS-CoV-WT (WT) or MERS-CoV-Δ4a (Δ4a) at an MOI of 3. (A) Whole cell lysates were prepared at 9 h p.i. and subjected to Western blot analysis to detect PKR, phosphorylated PKR (p-PKR), eIF2α, phosphorylated eIF2α (p-eIF2α), MERS-CoV 4a protein, MERS-CoV 4b protein, and tubulin. (B) HeLa/CD26 cells were radiolabeled for 1 h with 100 μCi of Tran^{35}S-label, and cell lysates were prepared at the indicated times p.i. Cell lysates were subjected to SDS-PAGE analysis, followed by autoradiography (top panels) and colloid Coomassie blue staining (bottom panels). Arrows depict virus-specific proteins. (C) Northern blot analysis of viral mRNAs using a riboprobe that binds to all viral mRNAs. Numbers 1-8 represent viral mRNA species. The 28S and 18S rRNAs were detected by ethidium bromide staining (rRNA). (D) Western blot analysis of intracellular accumulation of MERS-CoV S, M, N proteins, and tubulin. (E and F) HeLa/CD26 (E) or Vero cells (F) were infected with MERS-CoV-WT (WT) or MERS-CoV-Δ4a (Δ4a) at an MOI of 0.01 (left panels) or 3 (right panels). Culture supernatants were collected at the indicated times p.i., and virus titers were determined by plaque assay. Each dot represents mean virus titers (±standard deviation) from three wells. Asterisks represent statically significant differences in virus titers (P<0.05).

Figure 1 Nakagawa et. al.

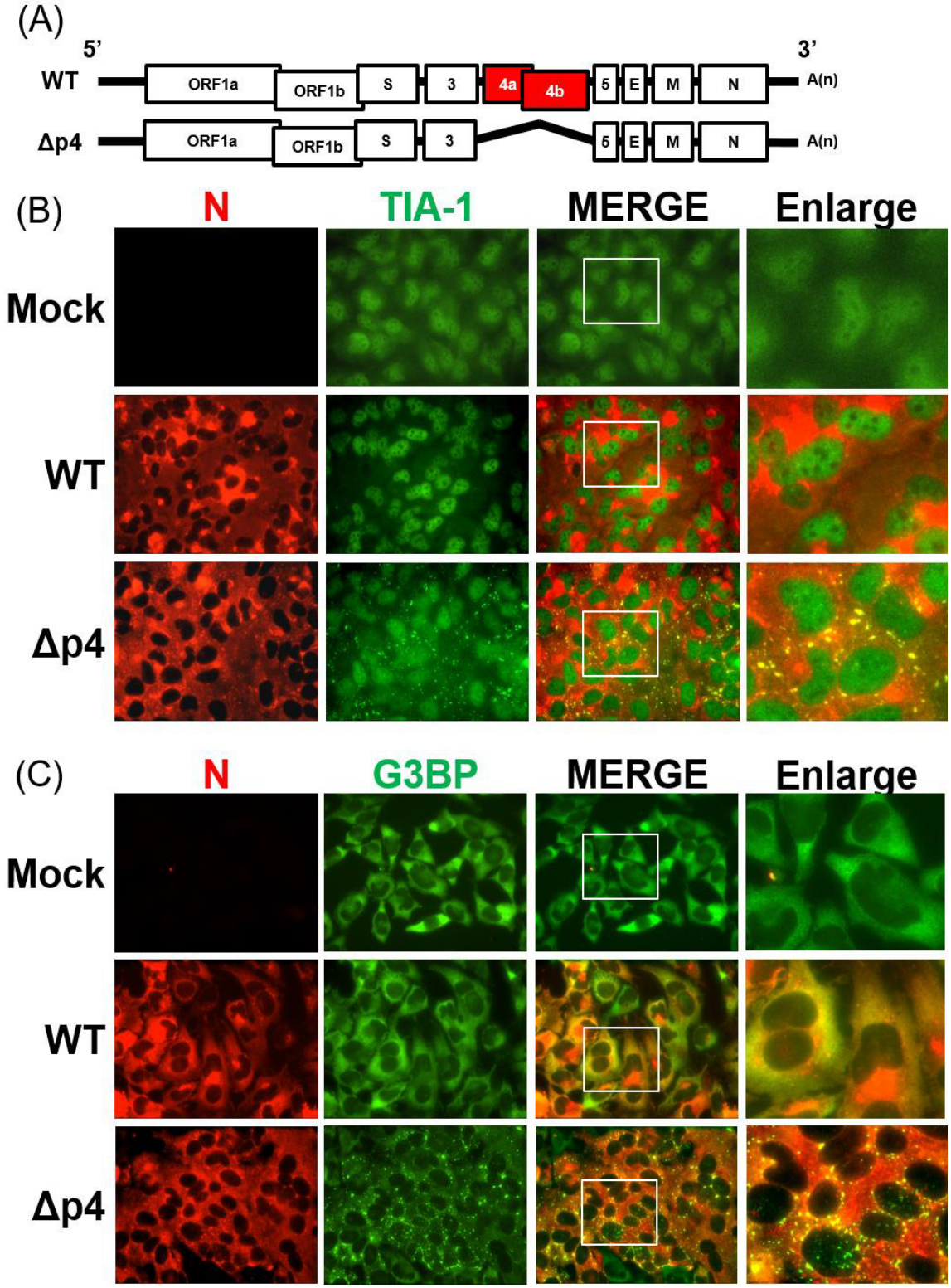

Figure 1 Nakagawa et. al.

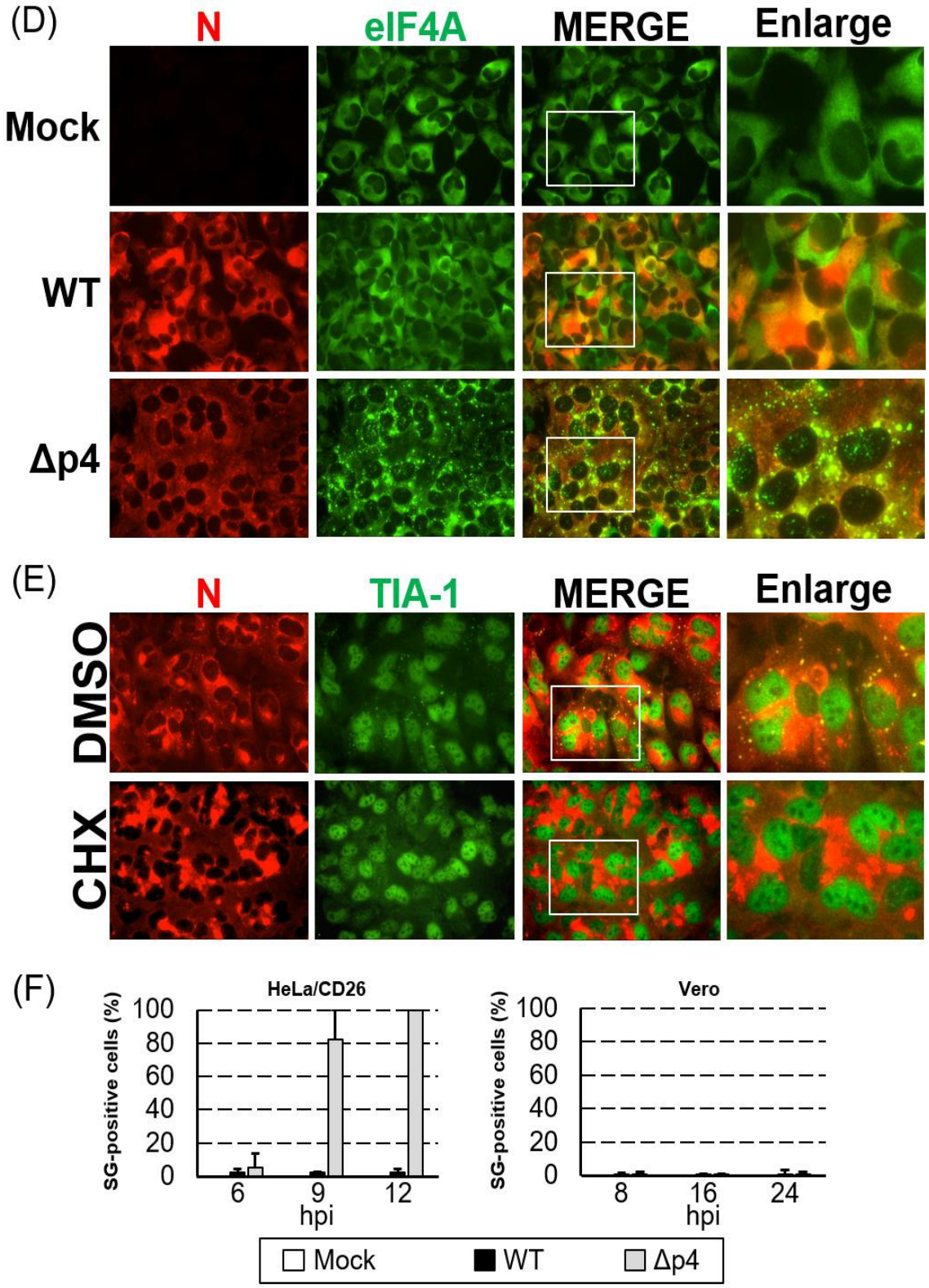

Figure 1 Nakagawa et. al.

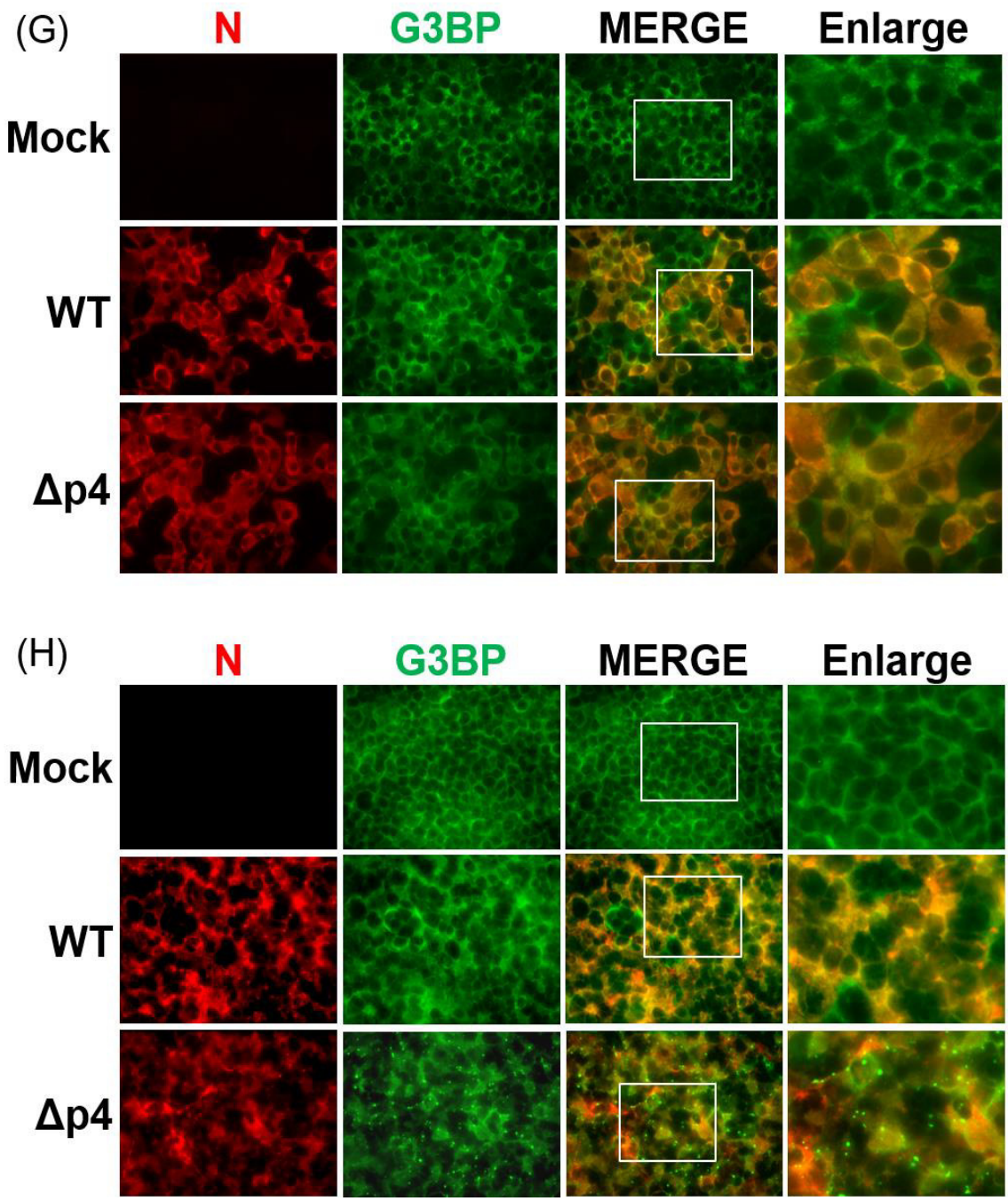

Figure 2 Nakagawa et. al.

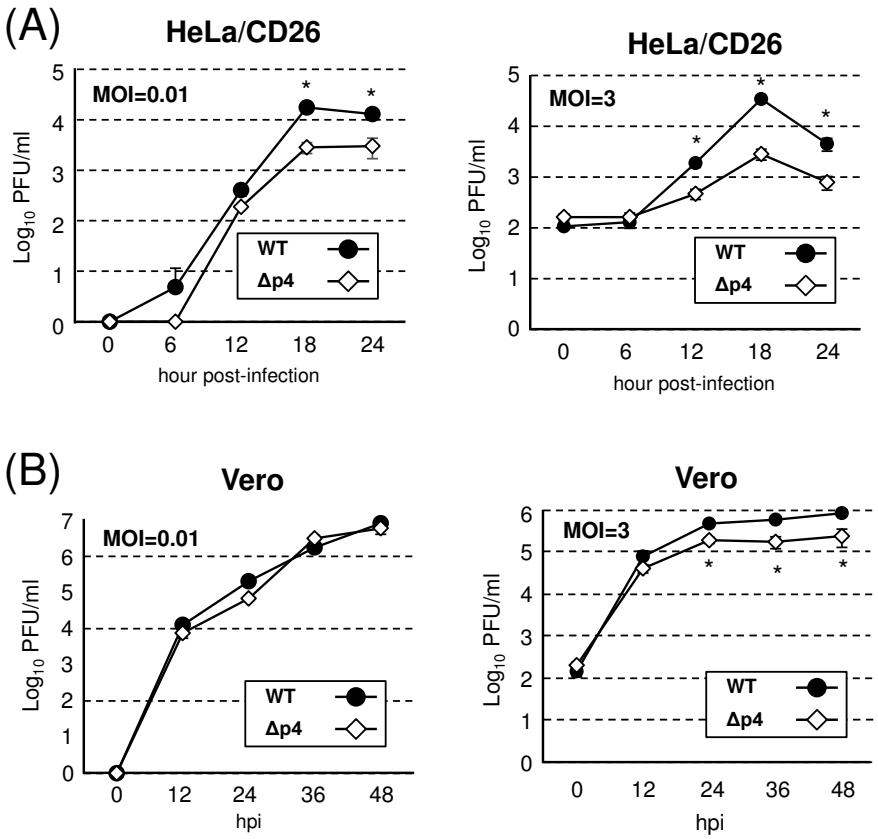

Figure 3 Nakagawa et. al.

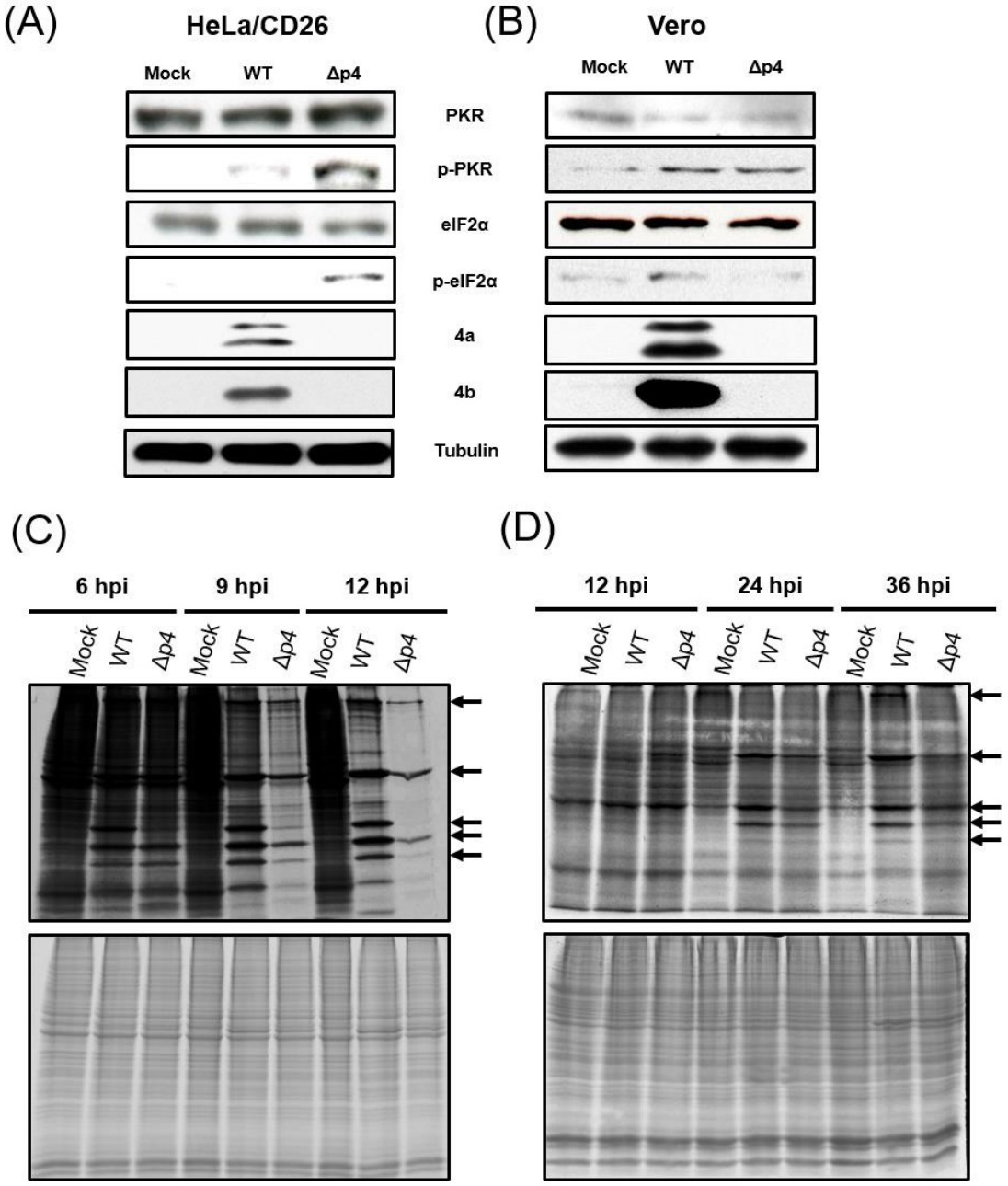

Figure 4 Nakagawa et. al.

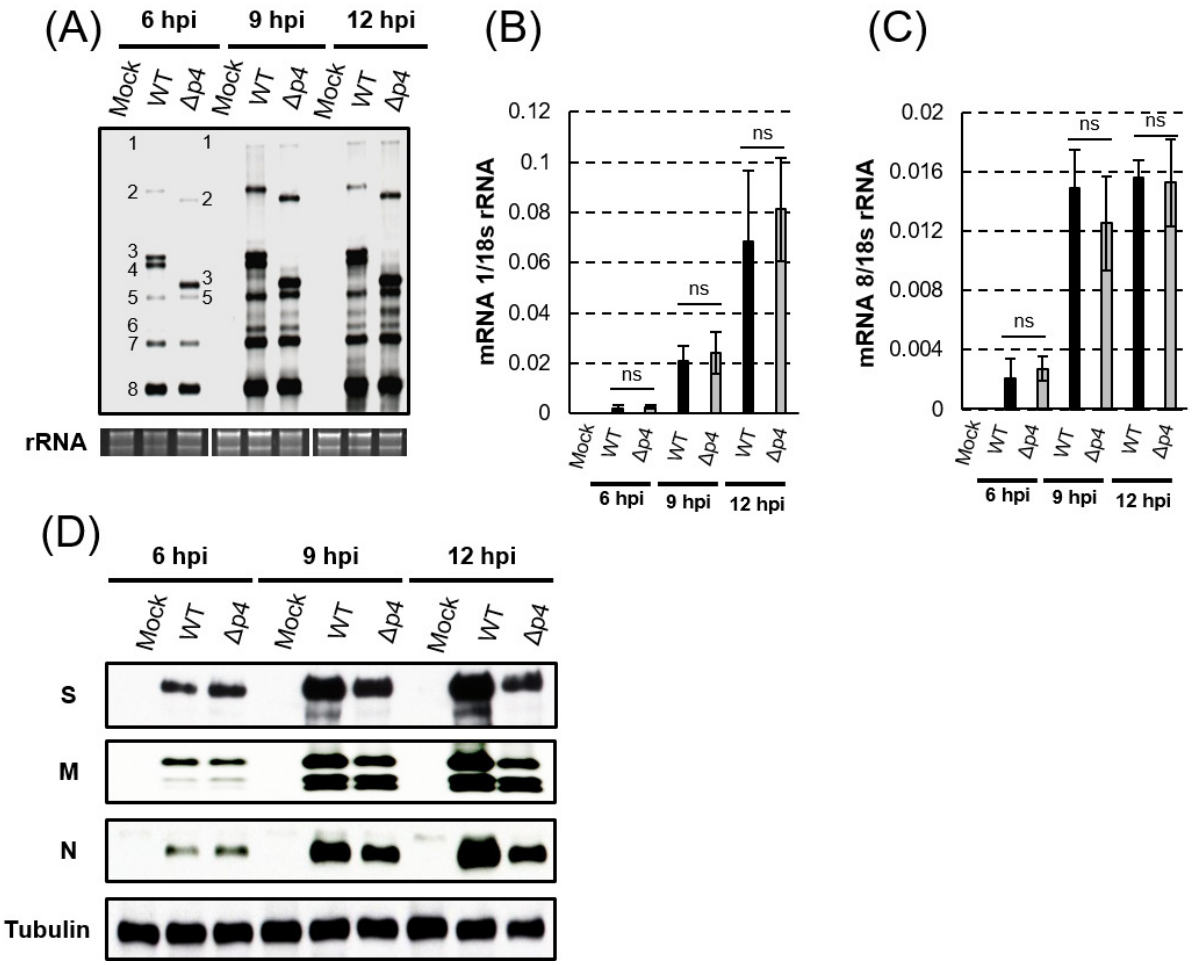

Figure 5 Nakagawa et. al.

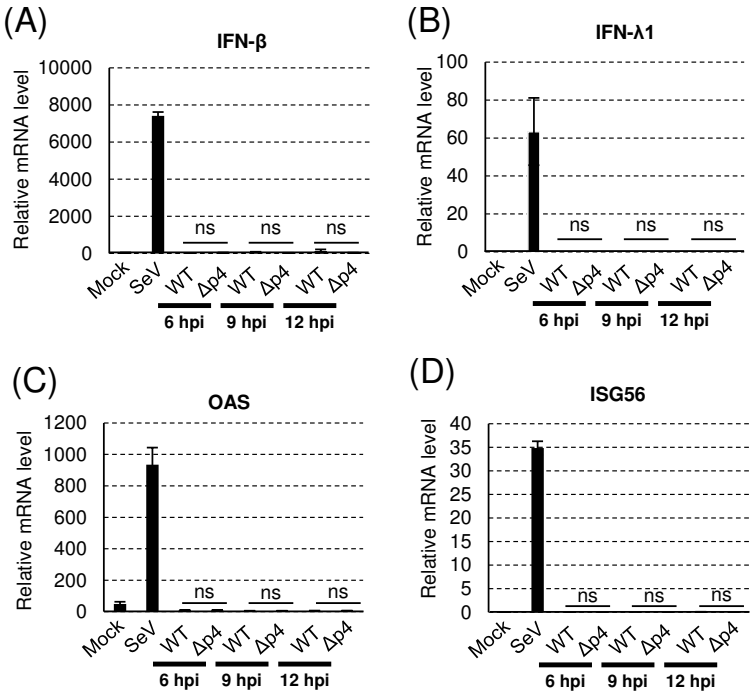

Figure 6 Nakagawa et. al.

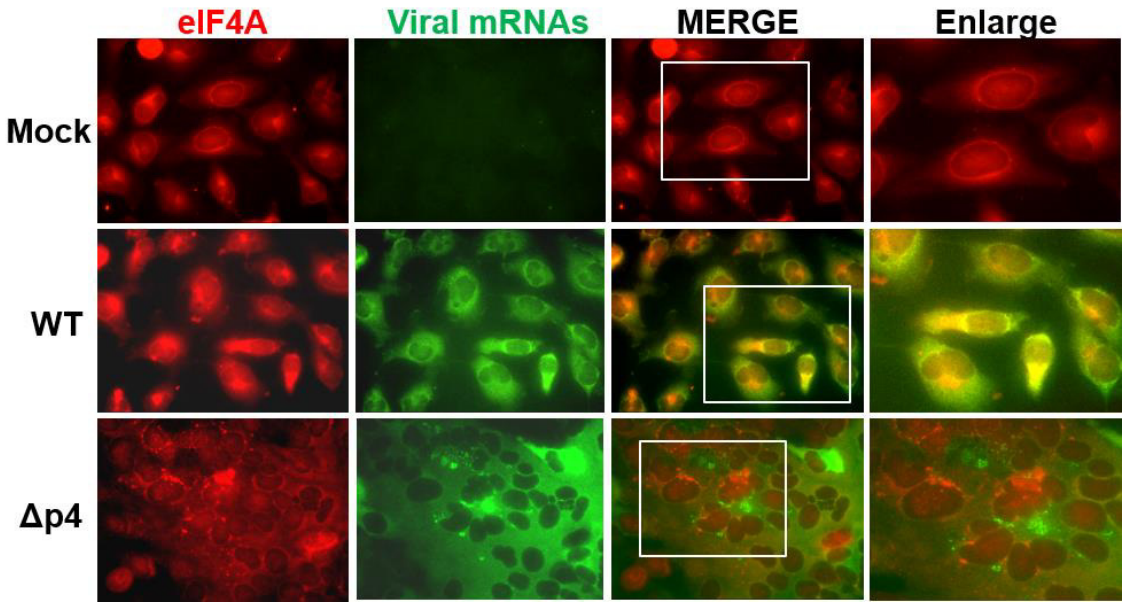

Figure 7 Nakagawa et. al.

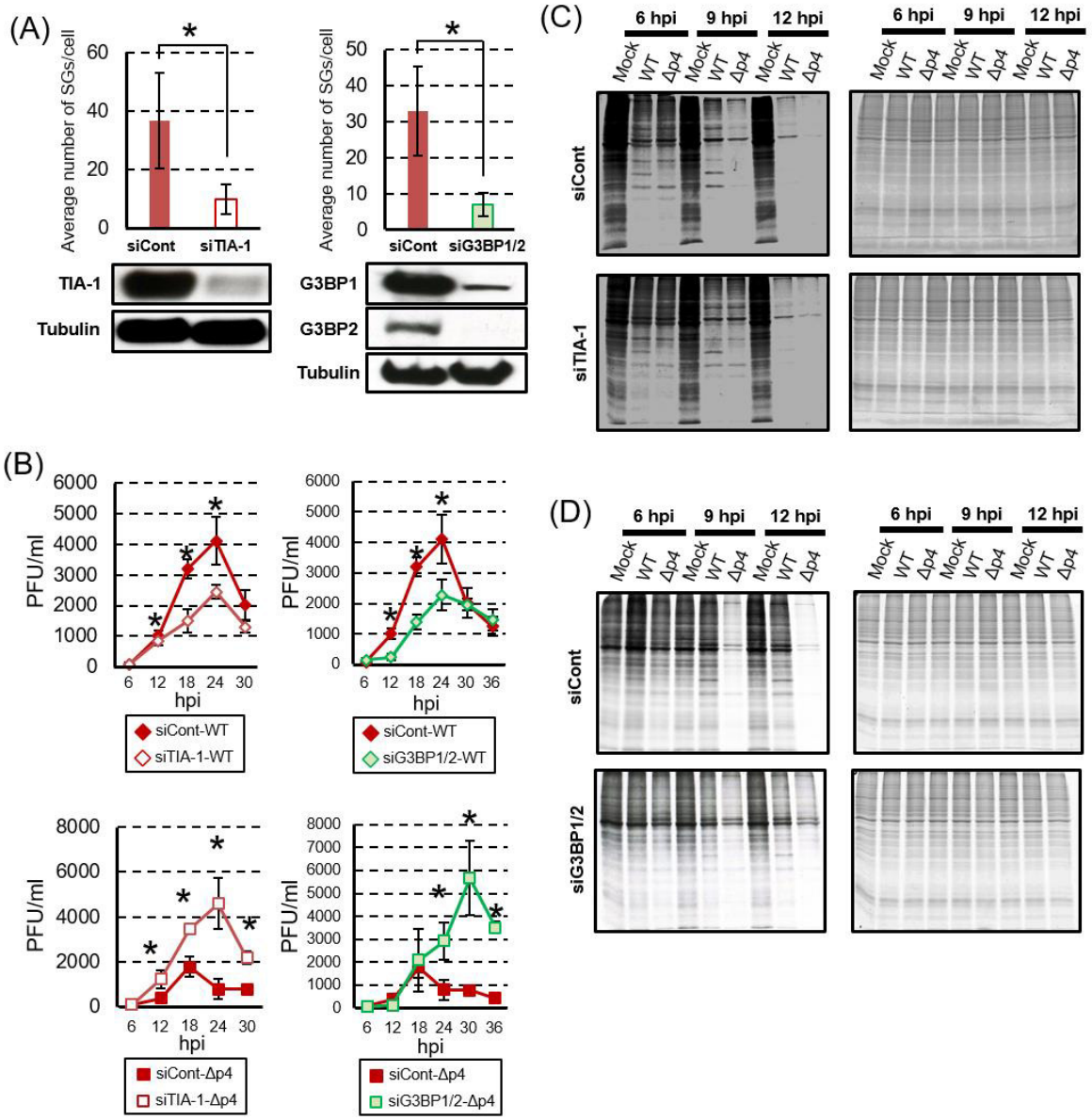

Figure 7 Nakagawa et. al.

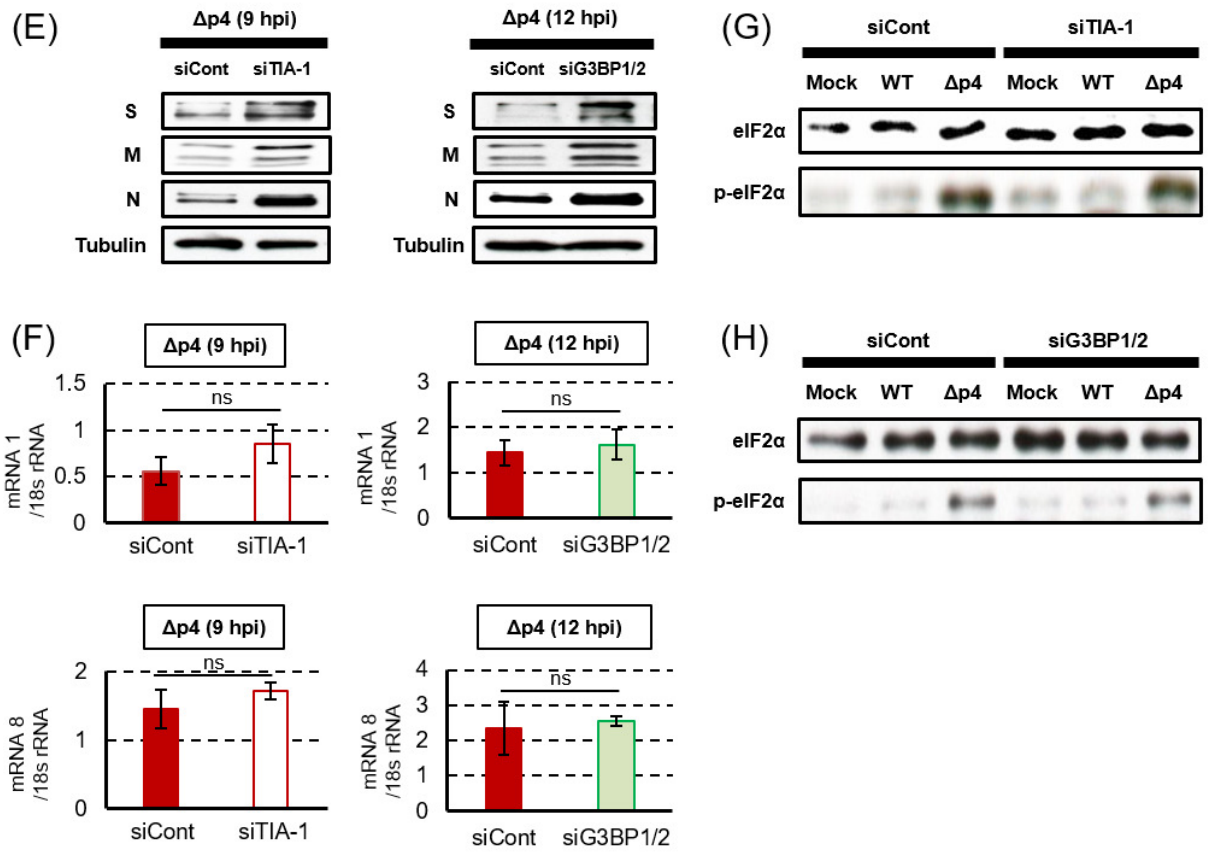

Figure 8 Nakagawa et. al.

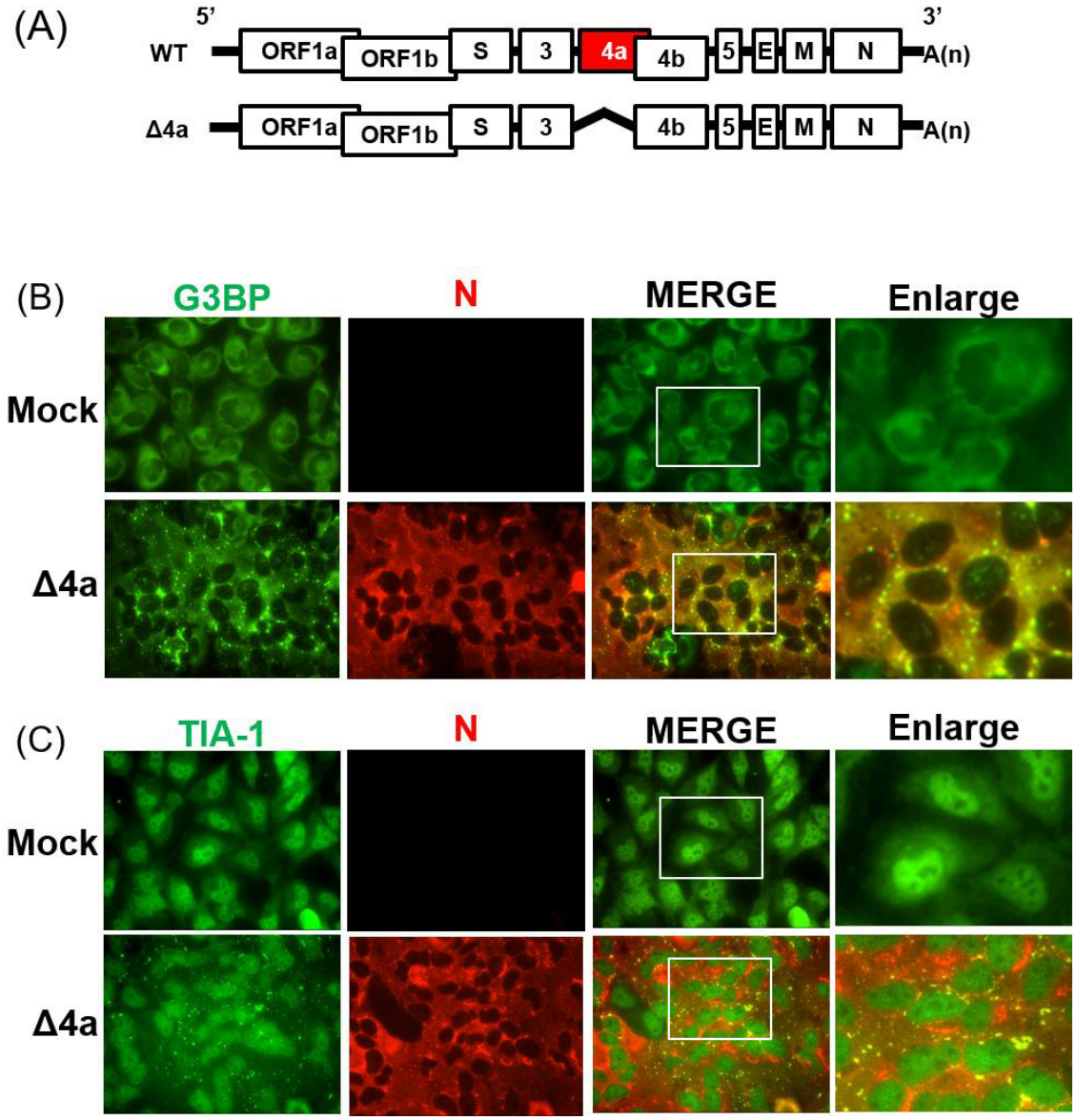

Figure 9 Nakagawa et. al.